© 2016. Published by The Company of Biologists Ltd | Development (2016) 143, 1055 doi:10.1242/dev.136507

CORRECTION

Reck enables cerebrovascular development by promoting canonical Wnt signaling

Florian Ulrich, Jorge Carretero-Ortega, Javier Menéndez, Carlos Narvaez, Belinda Sun, Eva Lancaster, Valerie Pershad, Sean Trzaska, Evelyn Véliz, Makoto Kamei, Andrew Prendergast, Kameha R. Kidd, Kenna M. Shaw, Daniel A. Castranova, Van N. Pham, Brigid D. Lo, Benjamin L. Martin, David W. Raible, Brant M. Weinstein and Jesús Torres-Vázquez

There were errors published in Development **143**, 147-159.

In the Funding section, grant [RSG-14045-01-DDC] should have been attributed to the American Cancer Society and not to the American Chemical Society. Tables S1 and S2 were missing from the supplementary data. These errors have been corrected online.

We apologise to the authors and readers for these mistakes.

© 2016. Published by The Company of Biologists Ltd | Development (2016) 143, 147-159 doi:10.1242/dev.123059

RESEARCH ARTICLE

Reck enables cerebrovascular development by promoting canonical Wnt signaling

Florian Ulrich[1,*], Jorge Carretero-Ortega[1,*], Javier Menéndez[1,*], Carlos Narvaez[1], Belinda Sun[1], Eva Lancaster[1], Valerie Pershad[1], Sean Trzaska[1], Evelyn Véliz[1], Makoto Kamei[2], Andrew Prendergast[3], Kameha R. Kidd[2], Kenna M. Shaw[2], Daniel A. Castranova[2], Van N. Pham[2], Brigid D. Lo[2], Benjamin L. Martin[4], David W. Raible[3], Brant M. Weinstein[2] and Jesús Torres-Vázquez[1,‡]

ABSTRACT

The cerebral vasculature provides the massive blood supply that the brain needs to grow and survive. By acquiring distinctive cellular and molecular characteristics it becomes the blood-brain barrier (BBB), a selectively permeable and protective interface between the brain and the peripheral circulation that maintains the extracellular milieu permissive for neuronal activity. Accordingly, there is great interest in uncovering the mechanisms that modulate the formation and differentiation of the brain vasculature. By performing a forward genetic screen in zebrafish we isolated *no food for thought* (*nft*^{y72}), a recessive late-lethal mutant that lacks most of the intracerebral central arteries (CtAs), but not other brain blood vessels. We found that the cerebral vascularization deficit of *nft*^{y72} mutants is caused by an inactivating lesion in *reversion-inducing cysteine-rich protein with Kazal motifs* [*reck*; also known as *suppressor of tumorigenicity 15 protein* (*ST15*)], which encodes a membrane-anchored tumor suppressor glycoprotein. Our findings highlight Reck as a novel and pivotal modulator of the canonical Wnt signaling pathway that acts in endothelial cells to enable intracerebral vascularization and proper expression of molecular markers associated with BBB formation. Additional studies with cultured endothelial cells suggest that, in other contexts, Reck impacts vascular biology via the vascular endothelial growth factor (VEGF) cascade. Together, our findings have broad implications for both vascular and cancer biology.

KEY WORDS: Angiogenesis, Blood-brain barrier, Brain vasculature, Reck, VEGF, Wnt

INTRODUCTION

The cerebral vasculature is essential for brain development, activity and homeostasis (Vallon et al., 2014). It supplies the metabolic needs of this organ, which consumes a fifth of the oxygen and a quarter of the glucose used by the body (Mergenthaler et al., 2013; Rolfe and Brown, 1997). Assembly of the cerebral vasculature involves endothelial cells initially found within vasculogenic perineural vessels. Some of these cells form angiogenic sprouts that invade the brain, yielding intracerebral vessels that branch and interconnect with the perineural vasculature (Ruhrberg and Bautch, 2013). Morphogenesis of the cerebral vasculature is accompanied by barriergenesis – the process of endothelial differentiation yielding the blood-brain barrier (BBB). Key BBB hallmarks include contiguous intercellular tight junctions, lack of fenestrations and selective or enriched expression of particular tight junction components and nutrient/efflux transporters (Hagan and Ben-Zvi, 2014; Obermeier et al., 2013; Siegenthaler et al., 2013). The BBB regulates the brain's extracellular ion balance, facilitates nutrient transport into the parenchyma, prevents the entrance of harmful molecules and metastatic cells, and enables neuroepithelial immune surveillance (Carson et al., 2006; Hawkins and Davis, 2005; Mergenthaler et al., 2013; Ousman and Kubes, 2012; Rolfe and Brown, 1997). Cerebral angiogenic growth and barriergenesis are modulated by neuroepithelial cues that activate endothelial signaling cascades (Hagan and Ben-Zvi, 2014). These include canonical Wnt or Wnt/β-catenin signaling, which promotes both aspects of vascular development specifically in the central nervous system (CNS), and global regulators of angiogenic growth that have positive (VEGF and SDF1) or negative (Notch and TGF-β) roles (Arnold et al., 2014; Bussmann et al., 2011; Fujita et al., 2011; Gridley, 2010; Larrivee et al., 2012; Mackenzie and Ruhrberg, 2012; Masckauchan and Kitajewski, 2006; Reis and Liebner, 2013). Reck (reversion-inducing cysteine-rich protein with Kazal motifs) is a dimeric multi-domain glycosylphosphatidylinositol (GPI)-anchored protein isolated as a tumor suppressor whose overexpression normalizes the aberrant morphology of transformed fibroblasts. Reck is an inhibitor for metalloproteinases (MPs) of the MMP (matrix metalloproteinase) and ADAM (A disintegrin and metalloproteinase) families (Chang et al., 2008; Hong et al., 2014; Nagini, 2012; Omura et al., 2009). MPs promote cell migration by weakening the mechanical barrier properties of the extracellular matrix (ECM) and reducing cell-cell adhesion by destruction of intercellular junctions (Page-McCaw et al., 2007; Seals and Courtneidge, 2003). For example, fly Reck limits basement membrane degradation (Srivastava et al., 2007) and glioma migration (Silveira Correa et al., 2010). MPs also modulate signaling pathways by cleaving ligands, receptors, ECM components (Page-McCaw et al., 2007; Seals and Courtneidge, 2003) and adherens junctions (Rims and McGuire, 2014). They can also act non-proteolytically (Mantuano et al., 2008; Mori et al., 2013). Accordingly, Reck also modulates cell signaling with MP dependency (Miki et al., 2010; Muraguchi et al., 2007). Finally, consistent with its multi-domain structure, Reck associates with the ERBB2 receptor to block its activity in an MP-independent fashion (Hong et al., 2011). Reck modulates the development of forelimbs, dorsal root ganglia neurons (DRG), brain (Muraguchi et al., 2007; Park et al., 2013; Prendergast et al., 2012; Yamamoto et al., 2012) and vasculature. *Reck*-knockout mice show perineural vascular plexus disorganization and reduced

[1]Dept of Cell Biology, Skirball Institute of Biomolecular Medicine, NYU Langone Medical Center, 540 First Avenue, New York, NY 10016, USA. [2]Program in Genomics of Differentiation, The Eunice Kennedy Shriver National Institute of Child Health and Human Development, National Institutes of Health, Bethesda, MD 20892, USA. [3]Department of Biological Structure, University of Washington, Seattle, WA 98195, USA. [4]Stony Brook University, Stony Brook, NY 11794, USA.
*These authors contributed equally.

‡Author for correspondence (torres@saturn.med.nyu.edu)

Received 26 February 2015; Accepted 25 November 2015

Development (2016) 143, 147-159 doi:10.1242/dev.123059

intracerebral vascularization (Chandana et al., 2010; Miki et al., 2010; Oh et al., 2001). In this study, we provide key mechanistic insights into how Reck modulates cerebrovascular development at both the cellular and molecular levels.

RESULTS

no food for thought mutants lack intracerebral blood vessels and DRG

In a zebrafish genetic screen (Shaw et al., 2006), we isolated the recessive-lethal mutant *nft*^{y72} for its brain-specific vascularization deficit. Although *nft*^{y72} mutants lacked intracerebral CtAs (Fig. 1A,B), its other cephalic blood vessels formed and carried circulation normally (Fig. 1A,B and Movies 1-4). Importantly, in the mutants, gross cerebral organization was undisturbed (Fig. S1). Cardiac contractility appeared normal (Movies 11,12). In the trunk, blood vessels formed and functioned properly (Fig. 1C,D and Movies 5-8) and the lymphatic thoracic duct was patterned correctly (Fig. 1F,H). However, the neural crest-derived DRG were missing (Fig. 1E,G). The shape, patterning and size of the head and body were unaffected (Fig. 1I-L), except for minor jaw defects (Prendergast et al., 2012).

nft^{y72} is a genetically null mutant allele of *reck*

nft^{y72} maps to a genetic interval spanning *Df(Chr24:reck)*^{w15} (chromosome 24 deficiency removing *reck* and other genes), which was isolated as a *sensory deprived* (*sdp;* now *reck*) allele in a screen for DRG-deficient mutants. All four *sdp* alleles are recessive lethal and genetic nulls (Prendergast et al., 2012). Given the positional and/or phenotypic similarities between *nft*^{y72}, *sdp* (Prendergast et al., 2012) and *Reck*-knockout (*Reck*$^{-/-}$) mice (Chandana et al., 2010) we tested *nft*^{y72} and *sdp* for complementation. We found that *nft*^{y72}/*sdp* transheterozygotes and both *nft*^{y72} and *sdp* homozygotes have large CtA and DRG deficits (Fig. S2A-H; Table S1). To compare *nft*^{y72} and *Df(Chr24:reck)*^{w15} with respect to additional cardiovascular phenotypes, see Fig. S2E-I, Fig. S3 and Movies 7-14.

DNA sequencing from *nft*^{y72} revealed a G-to-A transition at position 761 of the 2868 nt open reading frame of *reck* (Prendergast et al., 2012), yielding a missense, non-conservative substitution of the evolutionarily conserved Cys^{254} residue to Tyr at the fourth cysteine knot 4 (CK4; Fig. 2A). A similar Cys substitution occurs in *sdp*^{w13} at CK1 (Prendergast et al., 2012; Fig. S3). To confirm that this *reck* transition is the causative mutation in *nft*^{y72} mutants we provided exogenous wild-type (WT) *reck* mRNA to one-cell stage embryos from *nft*^{y72}/+ in-crosses (see Prendergast et al., 2012). This treatment rescued the CtA and DRG deficits of *nft*^{y72} (henceforth called *reck*^{y72}) mutants without yielding a surplus of these structures (Fig. 2B-F), indicating that *reck* plays permissive roles in the formation of CtAs and DRG. Together with the results of experiments using tissue-specific gene expression to rescue CtA formation in *reck*^{y72} mutants (Fig. 3, Figs S6, S11), the identical intracerebral vascularization deficits of *reck*^{y72} and *Df(Chr24:reck)*^{w15} mutant embryos (Fig. 3J) and the differential subcellular localization of the WT and Reck^{y72} mutant proteins (Fig. 2G-J), our observations imply that *reck*^{y72} is an amorphic allele of *reck*.

The mutant Reck^{y72} protein is inactive because it fails to reach the outer cell surface

Secretion of disulfide-bridged proteins is often impaired by Cys substitutions (Bodin et al., 2007; Boute et al., 2004; Claffey et al., 1995; Halliday et al., 1999; Mason, 1994; Schrijver et al., 1999). Thus, we hypothesized that the inactivity of Reck^{y72} is due to failure to reach the outer cell surface (see Simizu et al., 2005). We thus assayed the cell surface localization of epitope-tagged (3×FLAG and 2×HA) WT (Reck) and mutant (Reck^{y72}) zebrafish proteins in non-permeabilized immunofluorescently stained cells (Imhof et al., 2008). In 293T cells epitope-tagged Reck was detected at the cell surface (Fig. 2G-H; these proteins are active: Fig. 3, Fig. S6). By contrast, Reck^{y72} was undetectable at the cell surface (Fig. 2I,J). Quantification of COS7 cell lysates showed that the localization disparity was not due to differential abundance (Fig. 2K,L). We also co-expressed differentially tagged versions of Reck and Reck^{y72} and found that the WT form still localized correctly. Our findings thus provide a simple molecular explanation for the recessive amorphic

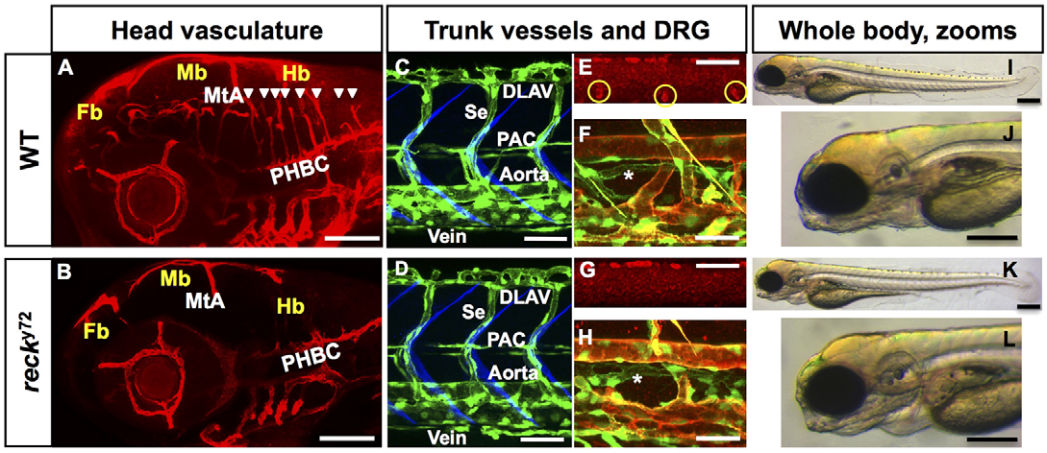

Fig. 1. *nft*^{y72} mutant embryos lack intracerebral blood vessels and DRG but have normal body morphology. Confocal (A-H) and bright-field (I-L) lateral images. Anterior, left; dorsal, up. A,B,E,G: 72 hpf; C,D: 48 hpf; F,H: 96 hpf; I-L: 60 hpf. (A,B) Central Arteries (CtAs) are found in WT (A) (white arrowheads) but are missing in *nft*^{y72} mutants (B); the other head vessels are present in *nft*^{y72}. Blood vessels [*Tg(kdrl:RFP)*^{s896}], red. WT (C) and *nft*^{y72} mutants (D) show identical trunk vascular patterns. Endothelium [*Tg(fli1a:eGFP)*^{y1}], green; somite boundaries, blue (Zygmunt et al., 2011). DRG (yellow circles; red HuC immunofluorescence) are present in WT (E) but absent in *nft*^{y72} mutants (G). (F,H) Blood vessels are green [*Tg(fli1a:eGFP)*^{y1}] and red [*Tg(kdrl:RFP)*^{s896}]; lymphatics (asterisks) are green only [*Tg(fli1a:eGFP)*^{y1}]. (J,L) Close-ups of head in I,K. MtA, metencephalic artery; PHBC, primordial hindbrain channel; DLAV, dorsal longitudinal anastomotic vessel; Se, intersegmental vessel; PAC, parachordal chain; Fb, forebrain; Mb, midbrain; Hb, hindbrain. Scale bars: 100 µm in A,B, 50 µm in C-E,G, 25 µm in F,H and 200 µm in I-L. See also Fig. S1, Movies 1-14 and Table S1.

Development (2016) 143, 147-159 doi:10.1242/dev.123059

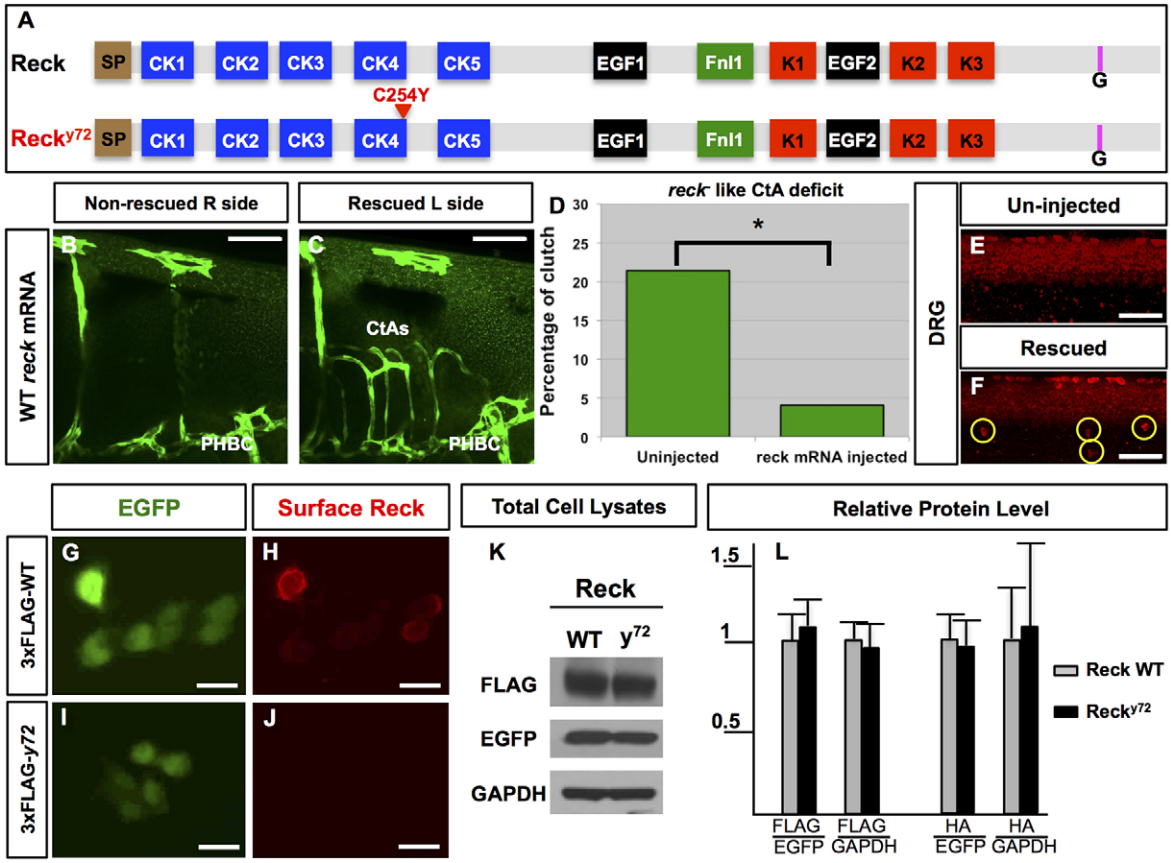

Fig. 2. *nft*^{y72} is a genetically null allele of *reck*. (A) WT zebrafish Reck (top) is 955 aa long and features the same domains and motifs found in mammalian RECK (Takahashi et al., 1998). N-terminal signal peptide (SP; brown), cysteine knot motifs (CK1-5; blue), epidermal growth factor-like repeats (EGF1-2; black), fibronectin-like type I module (Fnl1; green), Kazal motifs (K1-3; red), C-terminal GPI transferase cleaveage site (G; pink). Mutant Reck^{y72} (bottom) harbors a missense amino acid change in an evolutionarily conserved Cys residue within CK4. (B-F) Providing WT *reck* mRNA to *reck*^{y72} mutants restores formation of both CtAs (B-D) and DRG (E,F). Embryos with unilateral CtA rescue {B,C; endothelium, green [*Tg(fli1a:eGFP)*^{y1}]} or bilateral DRG rescue (F; yellow circles, red HuC immunofluorescence; only one side shown). Quantification of CtA rescue expressed as the percentage of embryos (from incrossing heterozygous mutant carriers) with *reck*$^{-}$-like CtA deficits (D). (G-L) Exogenous co-expression of epitope-tagged zebrafish Reck (WT Reck or mutant Reck^{y72}) with cytosolic EGFP in cultured mammalian cells. (G-J) Immunofluorescence-based detection of surface 3×FLAG-Reck (red) and EGFP fluorescence (green) in non-permeabilized 293T cells. 3×FLAG-Reck^{y72} fails to reach the cell surface (J). (K,L) WT and mutant Reck^{y72} expressed in COS7 cells show similar abundance. (K) Western blot of total cell lysates from cells expressing WT or mutant 3xFLAG-Reck. (L) Densitometry-based quantification total cell lysates from cells expressing WT Reck or mutant Reck^{y72} zebrafish proteins tagged with 3×FLAG or 2×HA. Protein levels normalized with EGFP and GAPDH. Error bars: s.e.m. Scale bars: 50 µm in B-C, 100 µm in E,F and 10 µm in G-J. See also Figs S2, S3, Movies 1-14 and Table S1.

nature of the *reck*^{y72} allele: Reck^{y72} fails to reach the outer cell surface without disrupting the targeting of its WT counterpart.

The intracerebral vascularization deficit of *reck*^{y72} mutants is due to decreased CtA-forming cell emigration

To elucidate the endothelial cellular bases of the intracerebral vascularization deficit of *reck* mutants (*reck*$^{-}$) we exploited the advantages of the hindbrain (Hb) vasculature as a model for cerebrovascular development, as we reported previously (Ulrich et al., 2011). The WT Hb harbors both extracerebral (perineural) and intracerebral vessels. These lie, respectively, ventral to the Hb or inside it (Fig. 4A). The extracerebral vasculature comprises the two lateral primordial hindbrain channels (PHBCs) and, at the midline, the posterior communicating segments (PCSs) and basilar artery (BA). The PHBCs communicate with the midline vessels via arteriovenous connections (avcs). The intracerebral vessels or CtAs sprout dorsally from the PHBCs into each rhombomere center. The assembly of the Hb vasculature at 24-72 hours post-fertilization (hpf) primarily involves endothelial cell migration and follows a reproducible sequence. The PHBCs and PCSs form first (Fig. 4B), then, PHBCs launch ventral sprouts towards the midline, which coalesce into the BA (Fig. 4C,D). While the BA forms, the CtAs emerge from the PHBCs, penetrate the Hb and connect to the PCS and BA (Fig. 4D,E). Most BA-forming sprout remnants are lost by 48 hpf; those that persist become avcs (Fig. 4D,E; see Bussmann et al., 2011; Corti et al., 2011; Fujita et al., 2011; Fukuhara et al., 2014; Isogai et al., 2001; Ulrich et al., 2011).

At the cellular level, the intracerebral vascularization deficit of *reck*$^{-}$ could be due to defects in the abundance and/or distribution of endothelial cells (Fig. 4F-K). Quantification of these parameters revealed that endothelial abundance was slightly reduced at 36 hpf but not at 50 hpf (Fig. 4J), consistent with a minor transient delay in the mutant's vascular development and eliminating the possibility that reduced endothelial cell abundance (as a result of impaired cell specification, proliferation and survival) causes the lack of CtAs in *reck*$^{-}$. By contrast, endothelial cell distribution was abnormal in the mutant: the PHBCs (but not the BA) were hyperplastic (Fig. 4J). We also found that *reck*^{y72} mutants had overabundant avcs (Fig. 4I,K,M), reminiscent of the murine perineural vascular plexus disorganization of *Reck*$^{-/-}$ embryos (Chandana et al., 2010).

Development (2016) 143, 147-159 doi:10.1242/dev.123059

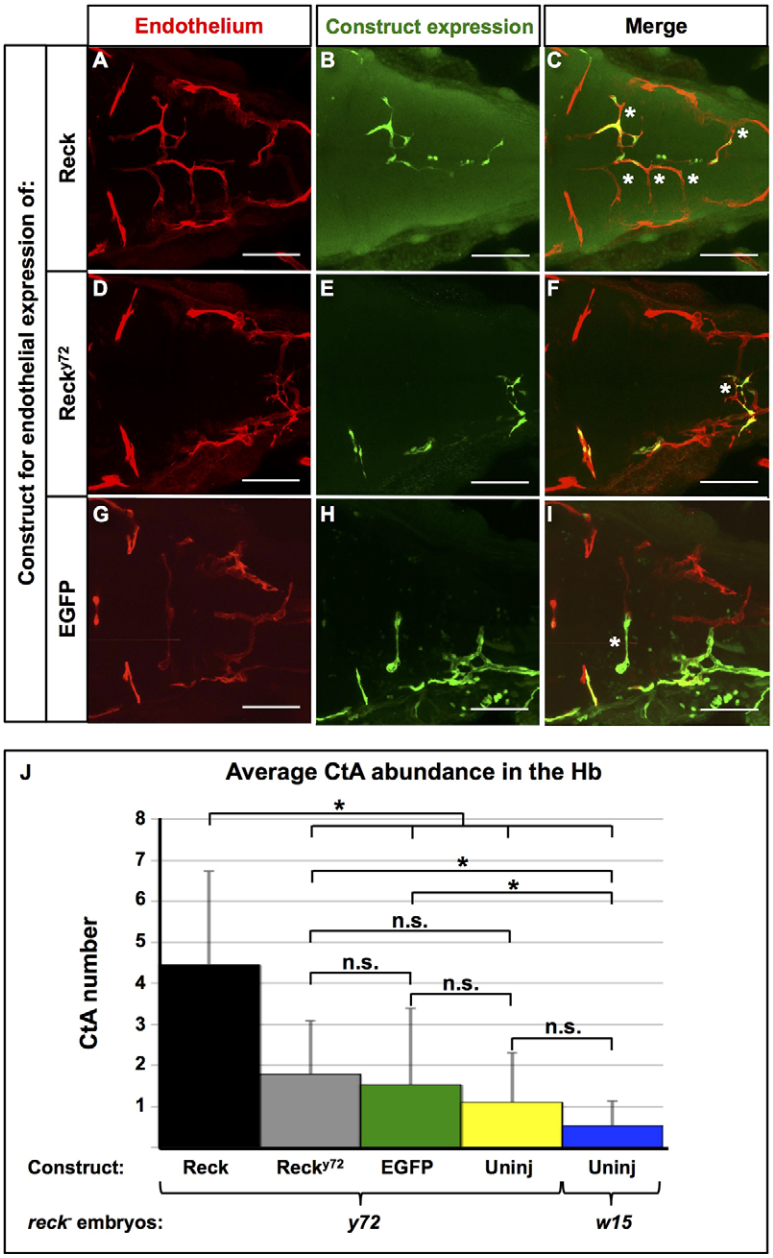

Fig. 3. Mosaic endothelial expression of WT Reck is sufficient to rescue the CtA deficit of *reck*^{y72} mutant embryos. (A-I) Dorsal views (dorsal level to show CtAs) of the 72 hpf Hb vasculature {red [*Tg(kdrl:RFP)*^{s896}]} of *reck*^{y72} injected with constructs driving endothelial expression of exogenous Reck, Reck^{y72} (both HA-tagged, see Fig. 2L) or EGFP proteins (green). Anterior, left; right side, up. (C,F,I) White asterisks indicate CtAs with exogenous expression of listed proteins. Scale bars, 100 µm. (J) Quantification of CtA abundance in the Hb of *reck*^{y72} and *Df(Chr24:reck)*^{w15} with or without ('Uninj') exogenous endothelial expression of listed proteins. Asterisks indicate significant differences (P<0.001); n.s., not significant; Student's t-test. *reck*^{y72} mutants scored: Reck (n=28), Reck^{y72} (n=14), EGFP (n=19), Uninj (n=20). *Df(Chr24:reck)*^{w15} mutants scored: Uninj (n=19). See also Fig. 4, Figs S6, S11.

Notably, the mutant avcs harbored only few cells (Fig. 4J). Together with the results of our time-lapse imaging showing that the PHBCs in *reck*^{y72} mutants failed to form CtA sprouts (Fig. S4 and Movies 15, 16), our observations indicate that the primary cellular defect leading to the intracerebral vascularization deficit of *reck*$^{-}$ is a dramatic reduction in CtA-forming endothelial cell emigration from the PHBCs, which, in turn, induce the hyperplasia of the latter (Fig. 4L,M).

reck limits the abundance of avcs, even without circulatory flow

Blood vessel perdurance and circulatory flow can be linked (Bussmann et al., 2011; Chen et al., 2012; Fish et al., 2008; Kochhan et al., 2013; Nicoli et al., 2010; Watson et al., 2013). For instance, drug-induced inhibition of the heartbeat reduces the abundance of avcs, which suggests that in WT embryos the few avcs that persist do so because they were carrying robust flow (Corti et al., 2011; Helisch and Schaper, 2003). Hence, we hypothesized that in *reck*$^{-}$, the CtA deficit increases circulatory pressure through extracerebral vessels (which have robust flow: Movies 1, 2, Table S1), secondarily enhancing maintenance and/or formation of avcs (Fig. S4, Movies 1, 2). We thus asked whether the overabundance of avcs in *reck*^{y72} mutants is suppressed by lack of circulatory flow. We abrogated cardiac contractility with *silent heart* (*sih*^{b109}), a recessive mutation that inactivates *cardiac troponin-t2a* (Sehnert et al., 2002). Unlike drug-based inhibition of circulatory flow, genetic abrogation of circulation increases the number of avcs, even in *reck*^{y72} mutants, and has little impact on the abundance of CtAs (Table S2 and Fig. S5; Bussmann et al., 2011; Corti et al., 2011; Fujita et al., 2011; Fukuhara et al., 2014; Isogai et al., 2001; Ulrich et al., 2011). Thus, *reck* limits the number of avcs, even without flow, strongly suggesting that the overabundance of avcs in *reck*^{y72} mutants is unrelated to circulatory pressure gains.

Development (2016) 143, 147-159 doi:10.1242/dev.123059

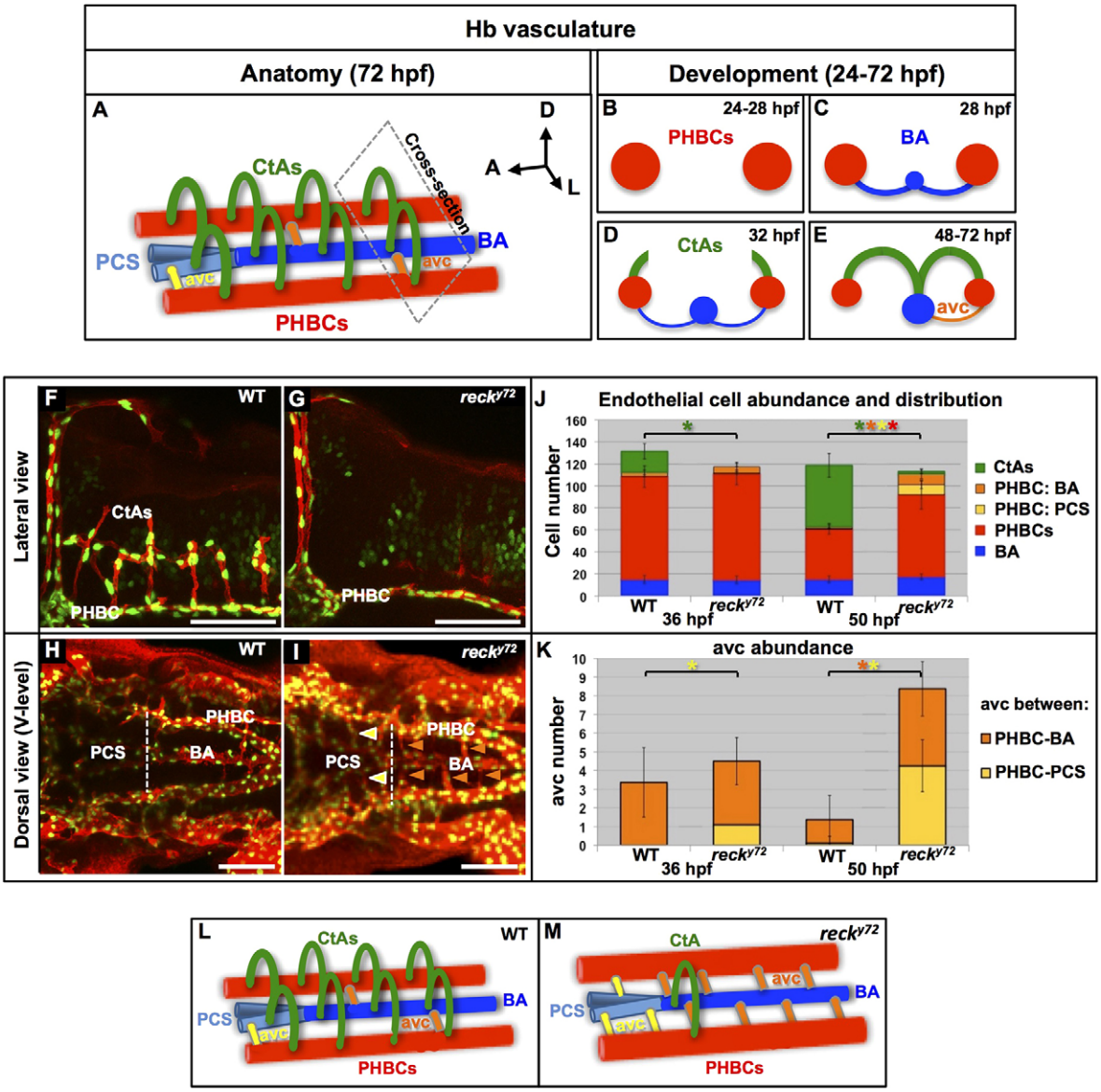

Fig. 4. CtA deficit in *reck*^{y72} mutant embryos is due to impaired endothelial cell migration from the perineural PHBCs. (A-E) WT Hb vasculature anatomy (A; anterior half detail) and development (B-E; cross-sections 'cut' along plane in A. Dorsal, up. PHBCs, red; BA, dark blue; PCS, light blue; avcs (PCS-connected, yellow; BA-connected, orange), CtAs; green. (F-K) Abundance and distribution of Hb endothelial cells and avcs at 36 and 50 hpf in WT and *reck*^{y72} embryos. (F-I) Confocal images (50 hpf). Endothelium, red [*Tg(kdrl:RFP)*^{s896}]; endothelial nuclei, green [*Tg(kdrl:eGFP-NLS)*^{zf109}]. Anterior, left. Scale bars: 100 µm. (F,G) Lateral views; dorsal, up. (H,I) Dorsal views (ventral level) of extracerebral vessels; left side, bottom. Arrowheads, avcs (PCS-connected, yellow; BA-connected, orange). (J,K) Quantification and distribution of endothelial cells (J) and abundance of avcs (K). Asterisks and bars are color matched. Asterisks indicate significant differences (P<0.001) between age-matched genotypes (Student's t-test). n=10 embryos per genotype and stage. Error bars indicate s.d. (L,M) Diagrams of the Hb vasculature phenotypes (anterior half detail) in WT (L) and *reck*^{y72} embryos (M). The mutant shows a dramatic CtA deficit, hyperplastic PHBCs and too many avcs. See also Figs S4, S5, Movies 15, 16 and Table S2.

reck is expressed in the cerebral endothelium where it is required non-cell autonomously for intracerebral vascularization

To visualize the cephalic expression of *reck* during cerebrovascular development we performed RNA *in situ* hybridization chain reaction (HCR; Choi et al., 2014) using 36 and 48 hpf WT embryos. Consistent with prior reports (Chandana et al., 2010; Miki et al., 2010; Prendergast et al., 2012), we found that in WT embryos, *reck* is expressed in cerebral vessels and neural crest derivatives. For example, at 48 hpf, *reck* expression was found in the MtA, PHBCs and CtAs, as well as the branchial arches (BAx; see Fig. 5A-C). On the basis of these observations, we hypothesized that development of CtAs requires *reck* activity in the cerebral endothelium. To test this hypothesis, we performed cell transplants between WT donors and *reck*^{y72} hosts, making chimeras with mosaicism in the Hb and/or its vessels (Carmany-Rampey and Moens, 2006). Although cell transplants rarely target the Hb endothelium, despite yielding frequent mosaicism in both the Hb and the trunk vasculature, we found that CtAs, like other vessels (Zygmunt et al., 2011), were of mixed clonal origin (Fig. 4D-F). Moreover, WT endothelial cells formed chimeric CtAs in *reck*^{y72} hosts (Fig. 5G; n=3 chimeras), consistent with the notion that intracerebral vascularization requires endothelial *reck* activity in a non-cell autonomous manner. Accordingly, mosaic endothelial expression of WT Reck (but not

Development (2016) 143, 147-159 doi:10.1242/dev.123059

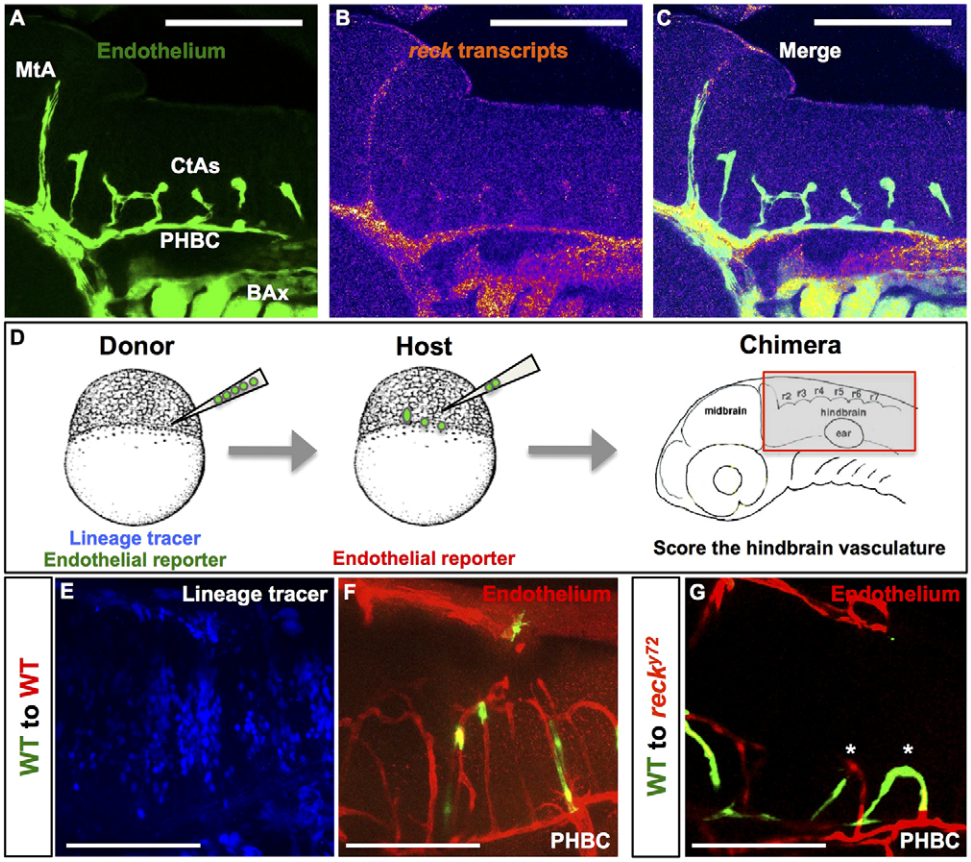

Fig. 5. *reck* is expressed in the cerebral endothelium where it is required non-cell autonomously for intracerebral vascularization. (A-C) Confocal lateral views of a 48 hpf WT Hb. Anterior, left; dorsal, up. (A) Endothelium is green [*Tg(fli1a:eGFP)*^{y1}]. (B) Fluorescent intensity of *reck* transcripts detected via RNA *in situ* HCR. Warmer and cooler colors represent, respectively, signals of higher and lower fluorescent intensity. *reck* is expressed in cerebral vessels (MtA, CtAs and PHBC) and BAx. (D) Workflow of cell transplantation experiments. Chimeras were analyzed at ~72 hpf. (E-G) Confocal lateral views of the Hb of two chimeras. Anterior, left; dorsal, up. Donor endothelium, green [*Tg(kdrl:EGFP)*^{1a116}]; host endothelium, red [*Tg(kdrl:RFP)*^{s896}]; lineage tracer, blue (Rhodamine 647 Dextran). (E,F) Chimera made using WT embryos. Note mosaicism in both the Hb environment (blue) and the CtAs (green and red). (G) Chimera made using a WT donor and a *reck*^{y72} host. Note mosaic CtAs (asterisks) containing both WT (green) and mutant (red) endothelial cells. Scale bars: 100 µm.

Reck^{y72} or EGFP) was sufficient to rescue the CtA deficit of *reck*^{y72} mutants (Fig. 3, Figs S6, S11).

reck is required for canonical Wnt signaling in the cerebral endothelium

The intracerebral vascular deficit of *reck*$^{-}$ best fits the model that Reck is a positive modulator of pathways that foster cerebral vascular development (Wnt, VEGF, SDF1) and/or an inhibitor of cascades that antagonize it (Notch, TGF-β). Since our experiments eliminated the latter possibility, we focused on testing the hypothesis that Reck promotes Wnt, VEGF and/or SDF1 signaling. We visualized the expression of molecular markers in WT and *reck*^{y72} mutants, including components and/or targets of these pathways. We found no obvious differences between genotypes in the neuroepithelial expression of genes encoding Wnt (*wnt1*), VEGF-A (*vegfaa* and *vegfab*) and SDF (*sdf1b*; also known as *cxcl12b*) ligands and Reck-targeted MPs (*mmp2* and *mmp14a*). Analysis of the expression of pan-endothelial genes [*fli1a*, *tie1* and *ve-cdh* (also known as *cdh5*)] and markers of specific cerebral vessels (*dab2*, *dll4* and *cxcr4a*) failed to reveal any obvious expression abnormalities, beyond the anticipated CtA labeling deficit in *reck*^{y72} mutants (Amoyel et al., 2005; Bai et al., 2005; Brown et al., 2000; Bussmann et al., 2011; Fujita et al., 2011; Janssens et al., 2013; Larson et al., 2004; Lyons et al., 1998).

However, consistent with the cerebrovascular role and expression of *reck* (Fig. 1A,B, Figs 3, 5, Fig. S6), we found that *reck*^{y72} mutants displayed abnormalities in the expression of both artificial and endogenous targets of the canonical Wnt signaling pathway in the cerebral endothelium (Figs 6, 7). For example, in WT embryos, the fluorescent reporter of canonical Wnt signaling *Tg(7xTCF-Xla.Siam:GFP)*^{ia4} (Moro et al., 2013) was expressed both in brain vessels (PHBCs and nascent CtAs at 36 hpf; CtAs at 48 hpf) and non-vascular cephalic tissues. By contrast, *reck*^{y72} embryos displayed a selective loss of cerebrovascular expression of *Tg(7xTCF-Xla.Siam:GFP)*^{ia4} (Fig. 6A-N″).

In addition, *reck*^{y72} mutants show altered expression of two genes that are endogenous targets of canonical Wnt signaling in the mammalian cerebral endothelium and serve as markers of BBB differentiation: *glucose transporter 1* (*glut1*, also known as *slc2a1a/b*) and *plasmalemma vesicle-associated protein* (*plvap*, also known as *vsg1*) (Fig. 7). Glut1 is a BBB component with Wnt-activated expression and *plvap* encodes a Wnt-repressed marker of fenestrated endothelium that highlights the immature BBB (Daneman et al., 2009; Hallmann et al., 1995; Liebner et al., 2008; Posokhova et al., 2015; Qian et al., 2005; Tam et al., 2012; Zhou and Nathans, 2014; Zhou et al., 2014). We found that at 72 hpf, Glut1 immunostaining labeled the MtA, PHBCs and CtAs of WT embryos (Fig. 7A-D″), but in *reck*^{y72} mutants, Glut1 was undetectable in the PHBCs, despite the fact that it remained in the MtA (Fig. 7E-G″). Conversely, *plvap* mRNA was found in the dorsal aspect of the CtAs, but not the extracerebral PHBCs in WT embryos at 48 hpf (Fig. 7H). However, in *reck*^{y72} embryos, the PHBCs displayed ectopic *plvap* expression (Fig. 7I).

We next asked whether the intracerebral vascularization deficits and aberrant expression of BBB-related markers found in *reck*^{y72} mutants can be phenocopied by inactivation of canonical Wnt signaling in otherwise WT embryos. To do this, we used transgenes that enable heat-induced global inhibition of canonical Wnt signaling by distinct mechanisms. *Tg(hsp70l:Xla.TCFΔC-EGFP)* drives expression of a dominant-negative form of the transcription factor TCF3 (T-cell factor 3; also known as LEF3) that lacks its DNA-binding HMG domain and is fused to EGFP. These truncated

Development (2016) 143, 147-159 doi:10.1242/dev.123059

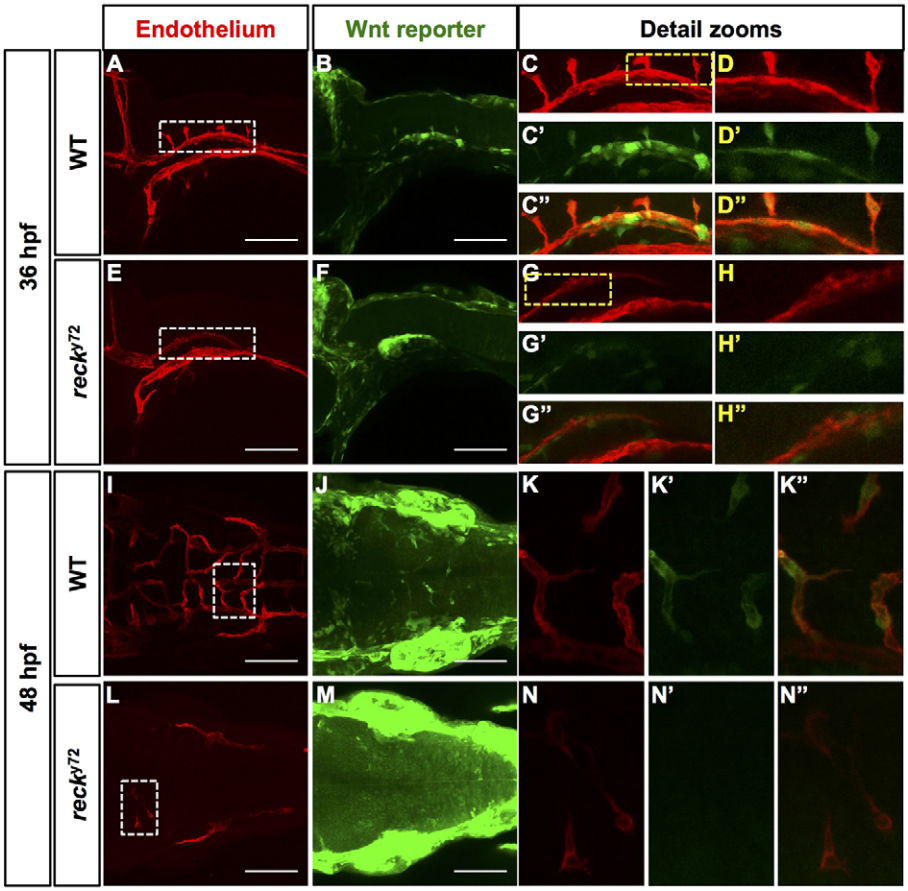

Fig. 6. The cerebrovascular expression of the transgenic reporter of canonical Wnt signaling *Tg(7xTCF-Xla.Siam:GFP)^{ia4}* is specifically lost in *reck^{y72}* mutant embryos. (A-N″) Confocal images (anterior, left) of 36 and 48 hpf Hbs from WT and *reck^{y72}*. Views: lateral (A-H″; dorsal, up); dorsal (I-N″; right side, up). Endothelium, red [*Tg(kdrl:RFP)^{s896}*]; Wnt reporter, green [*Tg(7xTCF-Xla.Siam:GFP)^{ia4}*]. In the WT, Wnt reporter expression highlights the PHBCs (A-D″), CtAs (A-D″,I-K″) and additional non-vascular tissues. However, in *reck^{y72}* mutants, expression of the Wnt reporter is undetectable in PHBCs (E-H″,L-N″) and occasional CtAs (N-N″), but is present elsewhere. Detail zooms: Regions in white dashed boxes (A,E,I,L) shown in C-C″,G-G″,K-K″ and N-N″, respectively; regions in yellow dashed boxes (C,G) shown in D-D″ and H-H″, respectively. See also Fig. 8.

forms of TCF3 (TCFΔC) act downstream of the destruction complex in Wnt-receiving cells by binding to β-catenin, preventing its interaction with endogenous TCF3 (Martin and Kimelman, 2012). *Tg(hsp70l:Mmu.Axin1-YFP)^{w35}* expresses a fusion of Axin1 (a pivotal component of the β-catenin destruction complex) and fluorescent YFP to promote β-catenin degradation (Kagermeier-Schenk et al., 2011; MacDonald et al., 2009; Stamos and Weis, 2013). We found that blocking canonical Wnt signaling with these tools yields defects in intracerebral angiogenesis and endothelial expression similar to those displayed by *reck^{y72}* mutants (Fig. S7). For example, forced expression of TCFΔC greatly inhibited CtA angiogenesis and abrogated Glut1 expression (Fig. S7E-H″) without disrupting the trunk's vascular patterning (Fig. S8). Similarly, Axin1-YFP reduced the abundance of CtA by ∼50% (Fig. S9E,F) and induced ectopic *plvap* expression in the PHBCs (Fig. S7J).

We also attempted to rescue CtA angiogenesis in *reck^{y72}* mutants by forced activation of canonical Wnt signaling. Briefly, we overexpressed constitutive active (ca) forms of β-catenin (caβ-catenin), either ubiquitously with the heat-inducible *Tg(hsp70l:caβ-catenin-2A-TFP)^{w130}* transgenic line (Veldman et al., 2013) or with endothelial specificity using *flt1*-driven mosaic expression (Wada et al., 2013; Wu et al., 2012; Yost et al., 1996). Forced expression of caβ-catenin inhibited CtA angiogenesis in WT animals and, unsurprisingly, failed to rescue CtA angiogenesis in *reck^{y72}* mutants. It is likely that in these experiments, the overexpression of caβ-catenin inhibited canonical Wnt signaling by transcriptional squelching (titration of endogenous transcription factors), as previously demonstrated (Prieve and Waterman, 1999). In addition, *flt1*-driven mosaic endothelial expression of a dominant-negative form of GSK3β (DN-GSK3-GFP; Taelman et al., 2010) had no effect on CtA angiogenesis in WT animals and failed to promote CtA angiogenesis in *reck^{y72}* mutants, consistent with the fact that chemical activation of Wnt signaling using the GSK3β inhibitors CHIR99021 and LiCl likewise failed to rescue both the DRG and CtA deficits of *reck^{y72}* mutants (Fig. S10; Klein and Melton, 1996; Ring et al., 2003; Vanhollebeke et al., 2015; Veldman et al., 2013). Overall, it is likely that the inability to achieve physiological levels of canonical Wnt signaling with proper spatio-temporal dynamics by forced expression of modified components of this pathway or with drugs explains why these treatments failed to rescue the defects of *reck^{y72}* mutants.

Nonetheless, our observations demonstrate that the role of canonical Wnt signaling in promoting intracerebral angiogenesis and proper expression of markers of barriergenic differentiation is evolutionarily conserved between zebrafish and mammals (Tam et al., 2012; Umans and Taylor, 2012). In addition, our other findings indicate that the cerebrovascular activity of canonical Wnt signaling is Reck dependent, thus uncovering this tumor suppressor as a key and novel modulator of this pathway.

Reck promotes VEGF signaling in cultured endothelial cells

VEGF signaling, which is crucial for intracerebral vascularization, is mediated primarily by receptors encoded by the zebrafish *kinase insert domain receptor-like* (*kdrl*) and mammalian *KDR* (also known as *VEGFR2*) 'ohnologs' (Bussmann et al., 2008; Habeck et al., 2002; Mackenzie and Ruhrberg, 2012; Sivaraj et al., 2013; Sohet and Daneman, 2013; Wittko-Schneider et al., 2013). We noted that the *kdrl* transcriptional reporters *Tg(kdrl:RFP)^{s896}* and/or *Tg(kdrl:GFP)^{1a116}* (Chi et al., 2008; Choi et al., 2007) were weakly expressed in PHBCs of *reck^{y72}* and *Df(Chr24:reck)^{w15}*

Development (2016) 143, 147-159 doi:10.1242/dev.123059

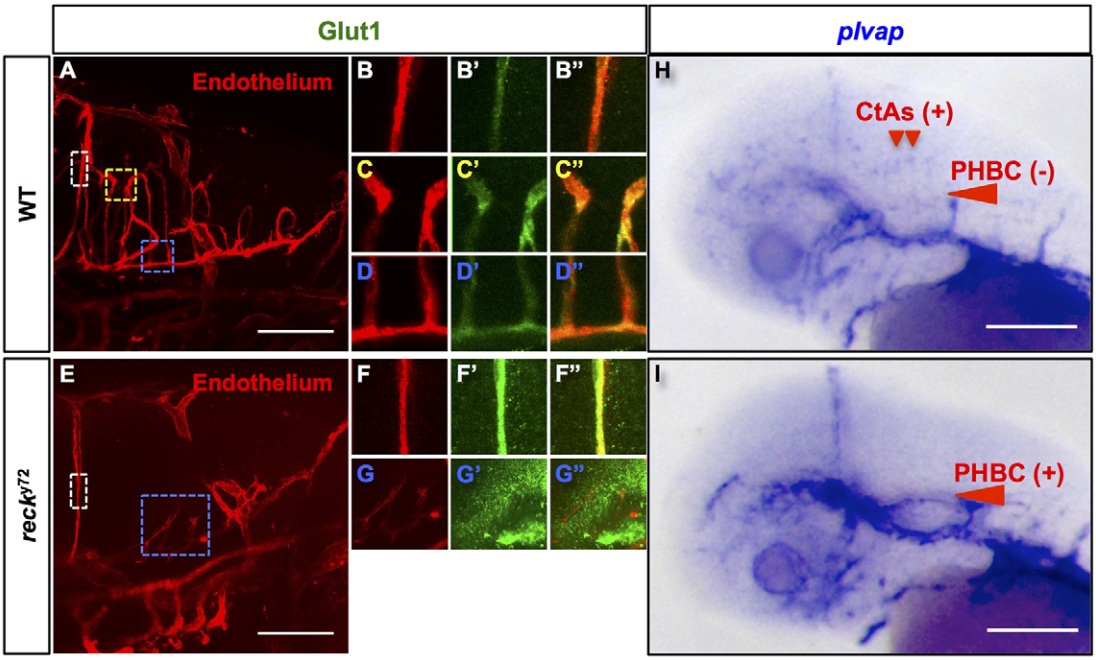

Fig. 7. *reck*^{y72} mutant embryos show aberrant cerebrovascular expression of the Wnt-responsive markers of barriergenic differentiation Glut1 and *plvap*. (A-G″) Confocal lateral images of the 72 hpf Hb vasculatures of WT (A-D″) and *reck*^{y72} embryos (E-G″). Anterior, left; dorsal, up. Endothelium, red [*Tg(kdrl:RFP)*^{s896}]; Glut1 immunofluorescence, green. Colored dashed boxes (A,E) demarcate a region of the following vessels: white, MtA (zooms: B-B″,F-F″); yellow, CtAs (zooms: C-C″); blue, PHBCs (zooms: D-D″,G-G″). Merged images of zooms are shown in B″,C″,D″,F″,G″. Glut1 decorates the MtA, CtAs and PHBCs of the WT (*n*=7 embryos). By contrast, Glut1 decorates the MtA, but not the PHBCs, of *reck*^{y72} (*n*=10 embryos). (H,I) Transmitted light images of the 48 hpf heads of embryos subjected to whole-mount RNA *in situ* hybridization with *plvap* riboprobes. (H) In the WT, *plvap* is expressed in the dorsal aspect of CtAs but not in the PHBCs (*n*=57 embryos). (I) In *reck*^{y72} mutants, *plvap* is ectopically expressed in the PHBCs (*n*=8 embryos). Scale bars: 100 µm. Merged images of detail zooms are shown in C″,D″,G″,H″,K″,N″. Scale bars: 100 µm. See also Figs S7-S9.

homozygotes, and *reck*^{y72}*/Df(Chr24:reck)*^{w15} trans-heterozygotes (Fig. S9A,B), but a similar reduction was not apparent in trunk vessels. By contrast, endothelial fluorescence from the *fli1a* transcriptional reporter *Tg(fli1a:EGFP)*^{y1} (Lawson and Weinstein, 2002) was unaffected in *reck*$^{-}$ embryos. We verified these qualitative observations by performing quantitative confocal imaging to determine the normalized fluorescent intensity (NFI) of *Tg(kdrl:RFP)*^{s896} using the signal of *Tg(fli1a:EGFP)*^{y1} as a reference (Venkiteswaran et al., 2013). These measurements confirmed that in *reck*^{y72} mutants, the fluorescence of *Tg(kdrl:RFP)*^{s896} decreased in the PHBCs, but not in other cephalic vessels such as the MtA (Fig. S9D). Consistent with the existence of distinct genetic circuits governing the activity of VEGF signaling in arterial and venous vessels (Covassin et al., 2006) we found that in CtA-deficient *kdrl*^{y17} mutants (Covassin et al., 2006) *Tg(kdrl:RFP)*^{s896} fluorescence was unaffected in the PHBCs but reduced in the MtA (Fig. S9C-D). These findings suggest that the expression of *kdrl* in the PHBCs, as in the trunk vessels (Wythe et al., 2013), is insensitive to VEGF signaling (but see also Lawson et al., 2003, 2002; Liang et al., 2001). We next overexpressed Axin1-YFP to determine whether inhibition of canonical Wnt signaling reduces *Tg(kdrl:RFP)*^{s896} expression (Veldman et al., 2013; Wang and Nakayama, 2009). Indeed, this treatment dramatically reduced *Tg(kdrl:RFP)*^{s896} expression (Fig. S9E,F). These observations

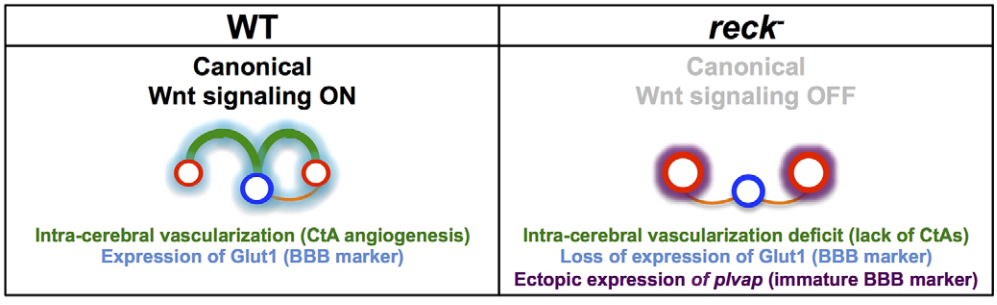

Fig. 8. Reck enables cerebrovascular canonical Wnt signaling to promote intracerebral vascularization and proper expression of barriergenesis markers. Hb vasculature cross-sections in WT and *reck*$^{-}$ embryos. Intracerebral CtAs, green. Extracerebral (perineural) vessels: PHBCs, red; BA, dark blue; avcs, orange. In WT animals (left), Reck ensures proper endothelial cell responsiveness to the canonical Wnt signals that promote CtA angiogenesis, induce cerebrovascular Glut1 expression (light blue) and repress *plvap* expression in the PHBCs. In *reck*$^{-}$ mutants (right), cerebrovascular canonical Wnt signaling is inactive, which dramatically impairs intracerebral vascularization, prevents Glut1 expression and induces ectopic expression of *plvap* in the PHBCs. *reck*$^{-}$ animals also show a disorganized perineural vessel network.

Development (2016) 143, 147-159 doi:10.1242/dev.123059

suggest that the cerebrovascular inactivation of canonical Wnt signaling in *reck*^{y72} mutants reduces *kdrl* expression, thereby secondarily impairing VEGF activity. Yet, additional observations are inconsistent with this possibility. First, the cerebrovascular phenotypes of *reck*$^{-}$ and *kdrl*$^{-}$ mutants are not identical. Both mutants lack CtAs, but in *kdrl* mutants, the BA is missing and cerebral endothelial abundance is reduced (Bussmann et al., 2011). Second, *plvap* was ectopically expressed in the PHBCs of *reck*^{y72} mutants (Fig. 7I) and in embryos in which canonical Wnt signaling was silenced by overexpression of Axin1-YFP (Fig. S7J). By contrast, in *kdrl*^{um19} mutants, *plvap* was not ectopically expressed (Fig. S9G-H). This finding is consistent with the emerging notion that intracerebral angiogenesis and barriergenic differentiation are genetically uncoupled (Hagan and Ben-Zvi, 2014) and suggests that VEGF activity is dispensable for cerebrovascular canonical Wnt signaling. Third, we found no obvious changes in the expression of VEGF-responsive markers such as *dll4*. Finally, RNA *in situ* HCR failed to reveal any obvious reduction in the abundance of *kdrl* transcripts in the cerebral vasculature of *reck*^{y72} mutants, but these were nearly undetectable in *kdrl*^{um19} mutants, probably as a result of nonsense-mediated mRNA decay (Brogna and Wen, 2009).

To investigate whether Reck can impact VEGF signaling in other contexts we used human umbilical vein endothelial cells (HUVECs) because they respond to VEGF and express *RECK* (Miki et al., 2010). In these experiments, we manipulated the availability of VEGF, the abundance of RECK and KDR kinase activity with the SU5416 inhibitor (Sakao and Tatsumi, 2011), we quantified VEGF signaling readouts (KDR, AKT and ERK1/2 phosphorylation levels) and measured the abundance of RECK and KDR (Fig. S9I-J′; Koch et al., 2011; Lanahan et al., 2013; Zachary, 2003). We found that knockdown of *RECK* impairs VEGF signaling by reducing pKDR and pAKT levels without affecting the abundance of pERK (Fig. S9I,J,I′), which is consistent with the different thresholds and kinetics of AKT and ERK phosphorylation (Olszewska-Pazdrak et al., 2009). Finally, knockdown of *RECK*, but not chemical abrogation of VEGF signaling, reduced the abundance of KDR (Fig. S9I-J′). Together, the results of our zebrafish and HUVEC studies suggest that Reck promotes VEGF signaling in contexts other than embryonic cerebrovascular development.

DISCUSSION

Our findings highlight Reck as a pivotal player in vascular development required for the branching morphogenesis and barriergenic differentiation of cerebral blood vessels (Fig. 8). At a cellular level *reck* acts in the first process by ensuring the migration-dependent formation of intracerebral vessels and remodeling of the perineural network. The results of our cell transplantation and tissue-specific *reck*^{y72} rescue experiments indicate that, consistent with its cerebrovascular expression pattern, *reck* is required in the brain endothelium in a non-cell autonomous manner to promote CtA angiogenesis (Chandana et al., 2010; Miki et al., 2010; Prendergast et al., 2012; Vanhollebeke et al., 2015).

Molecularly, *reck* is required for proper expression of *glut1* and *plvap*, two barriergenic differentiation markers regulated by canonical Wnt signaling. Accordingly, the cerebrovascular expression of a transgenic reporter of canonical Wnt signaling is lost in *reck*^{y72} mutants. Our study thus reveals that canonical Wnt signaling promotes intracerebral angiogenesis and barriergenic gene expression with evolutionarily conservation from fish to mammals (Daneman et al., 2009; Liebner et al., 2008; Posokhova et al., 2015; Tam et al., 2012; Zhou and Nathans, 2014; Zhou et al., 2014) and shows that Reck plays a pivotal role in enabling cerebrovascular canonical Wnt signaling (Vanhollebeke et al., 2015).

These novel mechanistic insights about *reck* might illuminate the etiology and treatment of CNS vascular diseases – such as familial exudative vitreoretinopathy (FEVR), osteoporosis-pseudoglioma syndrome (OPPG) and Norrie disease – that are caused by aberrant Wnt signaling and suggest strategies for manipulating vascular barriers to enable drug delivery into the CNS (Daneman et al., 2009; Dejana, 2010; Hagan and Ben-Zvi, 2014; Hawkins and Davis, 2005; Liebner et al., 2008; Obermeier et al., 2013; Siegenthaler et al., 2013; Vallon et al., 2014; Zhou et al., 2014). Accordingly, future studies will determine whether *reck*, like canonical Wnt signaling, regulates vascular development and/or maintenance throughout the CNS (Daneman et al., 2009; Liebner et al., 2008; Stenman et al., 2008).

How *reck* promotes canonical Wnt signaling remains undefined at the biochemical level. Reck associates with Gpr124, another novel member of the canonical Wnt signaling pathway that acts downstream of Wnt7 ligands, which has a role in cerebrovascular and DRG development similar to Reck (Posokhova et al., 2015; Vanhollebeke et al., 2015; Wang et al., 2014; Zhou and Nathans, 2014). Thus, Reck-Gpr124 heteromers might modulate Wnt7 binding, the assembly of the Wnt signaling complex, its internalization and/or MP-mediated processing events that gate its activity. However, it is worth highlighting that the effects of inactivating *reck* and *gpr124* are not fully equivalent. For example, *gpr124* mutants begin to recover intracerebral angiogenesis at 5 dpf and 50% of them survive to become adults without any apparent deficits in cerebral vascularization (Vanhollebeke et al., 2015). By contrast, in mutants of the different *reck* alleles, CtA angiogenesis does not recover after 5 dpf and lethality is fully penetrant by 10 dpf. Similarly, the CtA and DRG deficits of *gpr124* morphants (Vanhollebeke et al., 2015), but not of *reck*^{y72} mutants, can be rescued by chemical activation of Wnt signaling.

Finally, our zebrafish and endothelial cell culture studies suggest that Reck promotes VEGF signaling in contexts other than cerebrovascular development, consistent with the involvement of Gpr124 in VEGF-mediated tumor angiogenesis (Wang et al., 2014). RECK is expressed in tumor vessels (Clark et al., 2011; Miki et al., 2010; Oh et al., 2001; Rahmah et al., 2012) and epigenetically inactivated in human cancers. Reduced abundance of RECK is a poor prognosis tumor signature linked to high metastasis and short survival in patients with cerebral glioma, neuroblastoma and other tumors (Nagini, 2012; Noda and Takahashi, 2007). Given the involvement of both canonical Wnt and VEGF signaling in both tumor vascularization and metastasis (Carmeliet, 2005; Goel and Mercurio, 2013; Hu et al., 2009; Klaus and Birchmeier, 2008), our findings might also prove relevant in these pathological settings.

MATERIALS AND METHODS

Zebrafish lines

Zebrafish (*Danio rerio*) were handled under protocols approved by the New York University IACUC/IBC.

Transgenes

The following transgenic fluorescent reporters were used. Endothelial: *Tg(kdrl:RFP)*^{s896} (Chi et al., 2008), *Tg(kdrl:EGFP)*^{la116} (Anderson et al., 2008) *Tg(kdrl:eGFP-NLS)*^{zf109} (Blum et al., 2008), *Tg(fli1a:eGFP)*^{y1} (Lawson and Weinstein, 2002); erythrocytes: *Tg(gata1a:DsRed)*^{sd2} (Traver et al., 2003); DRG (and other neuronal populations): *Tg(neurog1:eGFP)*^{w61} (McGraw et al., 2008); canonical Wnt signaling activity: *Tg(7xTCF-Xla.Siam:GFP)*^{ia4} (Moro et al., 2013). Transgenes for inhibiting canonical Wnt signaling were *Tg(hsp70l:Mmu.Axin1-YFP)*^{w35}

Development (2016) 143, 147-159 doi:10.1242/dev.123059

(Kagermeier-Schenk et al., 2011) and *Tg(hsp70l:Xla.TCFΔC-EGFP)* (Martin and Kimelman, 2012). Transgene used for activating canonical Wnt signaling was *Tg(hsp70l:caβ−catenin-2A-TFP)*^{w130} (Veldman et al., 2013). Mutant transgenes used were *kdrl*^{y17} and *kdrl*^{um19} (Covassin et al., 2009; Meng et al., 2008), *reck*^{y72} (this study), *reck*^{w14} and *Df(Chr24:reck)*^{w15} (Prendergast et al., 2012), *sih*^{b109} (Sehnert et al., 2002). Genotyping protocols are provided in supplementary Materials and Methods.

Zebrafish heat-shock (HS) treatments for inducible inhibition or activation of canonical Wnt signaling

Tg(hsp70l:Xla.TCFΔC-EGFP), *Tg(hsp70l:caβ−catenin-2A-TFP)*^{w130} and their HS controls were heat-shocked at 40°C for 30 min at 30 hpf and fixed at 48 hpf. *Tg(hsp70l:Mmu.Axin1-YFP)*^{w35} and its HS controls were heat-shocked at 39°C for 1 h at 24 hpf and fixed and/or imaged live at 48 hpf. *Tg(hsp70l:Xla.TCFΔC-EGFP)* and *Tg(hsp70l:Mmu.Axin1-YFP)*^{w35} transgenes were provided paternally.

Antibodies

Primary antibodies used in zebrafish experiments: rabbit anti-RFP (1:500; Clonetech, 632496), rabbit anti-GFP (1:2000; Life Technologies, A11122), mouse anti-phospho-FAK y397 (1:100; Millipore, MAB1144), rabbit Glut1 (1:200; Novus Biologicals, NB300666), mouse zrf1 (1:10; ZIRC), mouse anti-3A10 (1:100; DSHB), mouse anti-HuC (1:100; Life Technologies, A21271) and mouse anti-HA (1:500; Cell Signaling, 2367S). Primary antibodies used in cell culture experiments purchased from Cell Signaling: pVEGFR-2 (1:1000; 2478), VEGFR-2 (1:5000; 2479), pAKT (Ser473; 1:1000; 4058), AKT (1:10,000; 9272), pERK1/2 (Ser473; 1:15,000; 4370), ERK1/2 (1:15,000; 4695), Reck (1:5000; 3433), GAPDH (1:10,000; 4058) and HA (1:10,000; 2367). GFP (1:5000; Life Technologies, A11121) and FLAG (1:20,000; Sigma, F1804) secondary antibodies were all used. Secondary antibodies for zebrafish and cell culture experiments were donkey Alexa Fluor-labeled anti-mouse or anti-rabbit antibodies from Life Technologies (1:1000; A31571, A10040, A21206 and A100036).

Phalloidin staining

Fixed embryos were incubated in a Phalloidin-488 (Sigma) solution for 2 h at room temperature as described by Snow et al. (2008).

Whole-mount RNA *in situ* hybridization (WISH)

Non-fluorescent chromogenic WISH was carried out as in Zygmunt et al. (2011). Fluorescent hybridization chain reaction (HCR-WISH) was performed as in Choi et al. (2014). See supplementary Materials and Methods for further details.

Cell culture experiments

HUVEC (Lifeline Cell Technology, FC-0003) cells were infected with anti-*RECK* shRNA lentiviral particles, puromycin-selected, starved overnight and stimulated with or without VEGFA. SU5416 (Sigma, S8442) was used for VEGFA signaling inhibition. HEK 293T (ATCC, CRL-11268) and COS-7 (ATCC, CRL-1651) cells were treated with Lipofectamine 2000 (Life Technologies) to transfect constructs for expressing epitope-tagged Reck and Reck^{y72}. Cells were tested for contamination by the commercial provider. Cells were used for western blotting or immunofluorescence studies 48 h post-transfection (see supplementary Materials and Methods for details).

Cell transplantation

Cell transplantation was carried out as previously described (Carmany-Rampey and Moens, 2006; Zygmunt et al., 2011).

Vectors for expressing Reck, Reck^{y72} (both epitope-tagged), EGFP, caβ-catenin and DN-GSK3-GFP in zebrafish and/or cultured cells

Tol2 transgenesis and *Tol2*/Gateway-based vectors were used for *flt1*-driven mosaic endothelial expression in zebrafish. Gateway-based vectors were used for CMV-driven expression in cultured cells (Bussmann et al., 2010; Hogan et al., 2009; Kwan et al., 2007; Villefranc et al., 2007).

reck^{y72} rescue via microinjection of WT *reck* mRNA

reck mRNA (100 pg) was injected into one-cell stage embryos.

Chemical activation of canonical Wnt signaling using GSK3β inhibitors

Dechorionated embryos were incubated with DMSO vehicle (0.7% in egg water; negative control) or GSK3β inhibitors starting at the 16-somite stage (16 hpf) until 72 hpf. The following GSK3β inhibitors were used: CHIR99021 (10 µM, diluted in DMSO) and LiCl (100 mM, diluted in egg water) as in Vanhollebeke et al. (2015) and Veldman et al. (2013).

Confocal microscopy and image processing

Image were acquired using a Leica SP5 confocal microscope with 40× dipping/water immersion objectives (NA=0.8 or 1.1), bi-directional scans at 200 lines/s in 1024×1024 pixel windows; *z*-stacks at 1 µm *z* intervals. Images are maximum intensity projections. Whole-head images were assembled from combining separately collected anterior and posterior regions using ImageJ and Photoshop. Live quantification of *Tg(kdrl:RFP)*^{s896} fluoresence in *Tg(kdrl:RFP)*^{s896}/+; *Tg(fli1a:eGFP)*^{y1}/+ embryos (WT and *reck*^{y72}) was carried out by normalizing RFP signals to those of GFP at every *z*-level with a custom ImageJ macro (Venkiteswaran et al., 2013), and the resulting values were averaged over all *z*-levels. Embryos were fixed in 1% agarose/PBS or fixed live at single time points in 1% agarose/fish medium with Tricaine and PTU or in 0.1% agarose under 1% agarose for live time-lapse imaging (Kaufmann et al., 2012; Lawson and Weinstein, 2002).

Statistical analysis

Densitometry data from western blot assays were analyzed using a two-tailed Student's *t*-test. Differences were considered significant when $P<0.05$. Error bars indicate s.e.m.

Acknowledgements

We thank David Kimelman, Deborah Yelon, Didier Stainier, Donghun Shin, Duc Si Dong, Eleanor Y. Chen, Edward De Robertis, Enrico Moro, Francesco Argenton, Gilbert Weidinger, H. Joseph Yost, James Amatruda, Jau-Nian Chen, Jeanot Muster, Jenna Galloway, Leonard Zon, Koichi Kawakami, Lilianna Solnica-Krezel, Markus Affolter, Michael Taylor Nathan Lawson, Richard Dorsky, Tatjana Piotrowski, Timothy Hla and Tohru Ishitani for zebrafish and/or reagents. Thanks to Harry Choi and Niles Pierce for HCR-WISH advice. We thank the Knaut lab and Michael Taylor for useful discussions and Dolly Chan, John Grosso and Wilberto Ortiz-Batista for administrative support.

Competing interests

The authors declare no competing or financial interests.

Author contributions

Genetic screen: B.D.L., B.M.W., D.A.C., J.T-V., K.M.S., K.R.K., M.K. and V.N.P. *nft*^{y72} mapping: B.D.L., D.A.C., V.N.P., and S.T. Zebrafish husbandry/genotyping: B.S., C.N. and E.L. *sdp* alleles, WT *reck* cDNA: A.P. and D.W.R. Designed/performed experiments: B.L.M., E.V., F.U., J.C.-O., J.M., and J.T.-V. Wrote the paper: J.T-V. All authors read, commented on and approved the manuscript.

Funding

Research was supported by a Consejo Nacional de Ciencia y Tecnología postdoctoral fellowship [187031 and 203862 to J.C.-O.], the American Heart Association [0735352N], the American Chemical Society [RSG-14045-01-DDC] and the National Institutes of Health [3R01HL092263-05S1-01A1 and 1R56HL118055-01A1] to J.T.-V. Deposited in PMC for release after 12 months.

Supplementary information

Supplementary information available online at
http://dev.biologists.org/lookup/suppl/doi:10.1242/dev.123059/-/DC1

References

Amoyel, M., Cheng, Y.-C., Jiang, Y.-J. and Wilkinson, D. G. (2005). Wnt1 regulates neurogenesis and mediates lateral inhibition of boundary cell specification in the zebrafish hindbrain. *Development* **132**, 775-785.

Anderson, M. J., Pham, V. N., Vogel, A. M., Weinstein, B. M. and Roman, B. L. (2008). Loss of unc45a precipitates arteriovenous shunting in the aortic arches. *Dev. Biol.* **318**, 258-267.

Arnold, T. D., Niaudet, C., Pang, M.-F., Siegenthaler, J., Gaengel, K., Jung, B., Ferrero, G. M., Mukouyama, Y.-S., Fuxe, J., Akhurst, R. et al. (2014). Excessive vascular sprouting underlies cerebral hemorrhage in mice lacking alphaVbeta8-TGFbeta signaling in the brain. *Development* **141**, 4489-4499.
Bai, S., Thummel, R., Godwin, A. R., Nagase, H., Itoh, Y., Li, L., Evans, R., McDermott, J., Seiki, M. and Sarras, M. P.Jr. (2005). Matrix metalloproteinase expression and function during fin regeneration in zebrafish: analysis of MT1-MMP, MMP2 and TIMP2. *Matrix Biol.* **24**, 247-260.
Blum, Y., Belting, H.-G., Ellertsdottir, E., Herwig, L., Lüders, F. and Affolter, M. (2008). Complex cell rearrangements during intersegmental vessel sprouting and vessel fusion in the zebrafish embryo. *Dev. Biol.* **316**, 312-322.
Bodin, L., Di Pasquale, E., Fabre, S., Bontoux, M., Monget, P., Persani, L. and Mulsant, P. (2007). A novel mutation in the bone morphogenetic protein 15 gene causing defective protein secretion is associated with both increased ovulation rate and sterility in Lacaune sheep. *Endocrinology* **148**, 393-400.
Boute, N., Zilberfarb, V., Camoin, L., Bonnafous, S., Le Marchand-Brustel, Y. and Issad, T. (2004). The formation of an intrachain disulfide bond in the leptin protein is necessary for efficient leptin secretion. *Biochimie* **86**, 351-356.
Brogna, S. and Wen, J. (2009). Nonsense-mediated mRNA decay (NMD) mechanisms. *Nat. Struct. Mol. Biol.* **16**, 107-113.
Brown, L. A., Rodaway, A. R. F., Schilling, T. F., Jowett, T., Ingham, P. W., Patient, R. K. and Sharrocks, A. D. (2000). Insights into early vasculogenesis revealed by expression of the ETS-domain transcription factor Fli-1 in wild-type and mutant zebrafish embryos. *Mech. Dev.* **90**, 237-252.
Bussmann, J., Lawson, N., Zon, L., Schulte-Merker, S. and **Zebrafish Nomenclature Committee**. (2008). Zebrafish VEGF receptors: a guideline to nomenclature. *PLoS Genet.* **4**, e1000064.
Bussmann, J., Bos, F. L., Urasaki, A., Kawakami, K., Duckers, H. J. and Schulte-Merker, S. (2010). Arteries provide essential guidance cues for lymphatic endothelial cells in the zebrafish trunk. *Development* **137**, 2653-2657.
Bussmann, J., Wolfe, S. A. and Siekmann, A. F. (2011). Arterial-venous network formation during brain vascularization involves hemodynamic regulation of chemokine signaling. *Development* **138**, 1717-1726.
Carmany-Rampey, A. and Moens, C. B. (2006). Modern mosaic analysis in the zebrafish. *Methods* **39**, 228-238.
Carmeliet, P. (2005). VEGF as a key mediator of angiogenesis in cancer. *Oncology* **69** Suppl. 3, 4-10.
Carson, M. J., Doose, J. M., Melchior, B., Schmid, C. D. and Ploix, C. C. (2006). CNS immune privilege: hiding in plain sight. *Immunol. Rev.* **213**, 48-65.
Chandana, E. P. S., Maeda, Y., Ueda, A., Kiyonari, H., Oshima, N., Yamamoto, M., Kondo, S., Oh, J., Takahashi, R., Yoshida, Y. et al. (2010). Involvement of the Reck tumor suppressor protein in maternal and embryonic vascular remodeling in mice. *BMC Dev. Biol.* **10**, 84.
Chang, C.-K., Hung, W.-C. and Chang, H.-C. (2008). The Kazal motifs of RECK protein inhibit MMP-9 secretion and activity and reduce metastasis of lung cancer cells in vitro and in vivo. *J. Cell. Mol. Med.* **12**, 2781-2789.
Chen, Q., Jiang, L., Li, C., Hu, D., Bu, J.-W., Cai, D. and Du, J.-L. (2012). Haemodynamics-driven developmental pruning of brain vasculature in zebrafish. *PLoS Biol.* **10**, e1001374.
Chi, N. C., Shaw, R. M., De Val, S., Kang, G., Jan, L. Y., Black, B. L. and Stainier, D. Y. R. (2008). Foxn4 directly regulates tbx2b expression and atrioventricular canal formation. *Genes Dev.* **22**, 734-739.
Choi, J., Dong, L., Ahn, J., Dao, D., Hammerschmidt, M. and Chen, J.-N. (2007). FoxH1 negatively modulates flk1 gene expression and vascular formation in zebrafish. *Dev. Biol.* **304**, 735-744.
Choi, H. M. T., Beck, V. A. and Pierce, N. A. (2014). Next-generation in situ hybridization chain reaction: higher gain, lower cost, greater durability. *ACS Nano* **8**, 4284-4294.
Claffey, K. P., Senger, D. R. and Spiegelman, B. M. (1995). Structural requirements for dimerization, glycosylation, secretion, and biological function of VPF/VEGF. *Biochim. Biophys. Acta* **1246**, 1-9.
Clark, J. C. M., Akiyama, T., Thomas, D. M., Labrinidis, A., Evdokiou, A., Galloway, S. J., Kim, H.-S., Dass, C. R. and Choong, P. F. M. (2011). RECK in osteosarcoma: a novel role in tumour vasculature and inhibition of tumorigenesis in an orthotopic model. *Cancer* **117**, 3517-3528.
Corti, P., Young, S., Chen, C.-Y., Patrick, M. J., Rochon, E. R., Pekkan, K. and Roman, B. L. (2011). Interaction between alk1 and blood flow in the development of arteriovenous malformations. *Development* **138**, 1573-1582.
Covassin, L. D., Villefranc, J. A., Kacergis, M. C., Weinstein, B. M. and Lawson, N. D. (2006). Distinct genetic interactions between multiple Vegf receptors are required for development of different blood vessel types in zebrafish. *Proc. Natl. Acad. Sci. USA* **103**, 6554-6559.
Covassin, L. D., Siekmann, A. F., Kacergis, M. C., Laver, E., Moore, J. C., Villefranc, J. A., Weinstein, B. M. and Lawson, N. D. (2009). A genetic screen for vascular mutants in zebrafish reveals dynamic roles for Vegf/Plcg1 signaling during artery development. *Dev. Biol.* **329**, 212-226.
Daneman, R., Agalliu, D., Zhou, L., Kuhnert, F., Kuo, C. J. and Barres, B. A. (2009). Wnt/beta-catenin signaling is required for CNS, but not non-CNS, angiogenesis. *Proc. Natl. Acad. Sci. USA* **106**, 641-646.
Dejana, E. (2010). The role of wnt signaling in physiological and pathological angiogenesis. *Circ. Res.* **107**, 943-952.
Fish, J. E., Santoro, M. M., Morton, S. U., Yu, S., Yeh, R.-F., Wythe, J. D., Ivey, K. N., Bruneau, B. G., Stainier, D. Y. R. and Srivastava, D. (2008). miR-126 regulates angiogenic signaling and vascular integrity. *Dev. Cell* **15**, 272-284.
Fujita, M., Cha, Y. R., Pham, V. N., Sakurai, A., Roman, B. L., Gutkind, J. S. and Weinstein, B. M. (2011). Assembly and patterning of the vascular network of the vertebrate hindbrain. *Development* **138**, 1705-1715.
Fukuhara, S., Zhang, J., Yuge, S., Ando, K., Wakayama, Y., Sakaue-Sawano, A., Miyawaki, A. and Mochizuki, N. (2014). Visualizing the cell-cycle progression of endothelial cells in zebrafish. *Dev. Biol.* **393**, 10-23.
Goel, H. L. and Mercurio, A. M. (2013). VEGF targets the tumour cell. *Nat. Rev. Cancer* **13**, 871-882.
Gridley, T. (2010). Notch signaling in the vasculature. *Curr. Top. Dev. Biol.* **92**, 277-309.
Habeck, H., Odenthal, J., Walderich, B., Maischein, H.-M., Schulte-Merker, S. and **Tubingen 2000 Screen Consortium**. (2002). Analysis of a zebrafish VEGF receptor mutant reveals specific disruption of angiogenesis. *Curr. Biol.* **12**, 1405-1412.
Hagan, N. and Ben-Zvi, A. (2014). The molecular, cellular, and morphological components of blood-brain barrier development during embryogenesis. *Semin. Cell Dev. Biol.*
Halliday, D., Hutchinson, S., Kettle, S., Firth, H., Wordsworth, P. and Handford, P. A. (1999). Molecular analysis of eight mutations in FBN1. *Hum. Genet.* **105**, 587-597.
Hallmann, R., Mayer, D. N., Berg, E. L., Broermann, R. and Butcher, E. C. (1995). Novel mouse endothelial cell surface marker is suppressed during differentiation of the blood brain barrier. *Dev. Dyn.* **202**, 325-332.
Hawkins, B. T. and Davis, T. P. (2005). The blood-brain barrier/neurovascular unit in health and disease. *Pharmacol. Rev.* **57**, 173-185.
Helisch, A. and Schaper, W. (2003). Arteriogenesis: the development and growth of collateral arteries. *Microcirculation* **10**, 83-97.
Hogan, B. M., Bos, F. L., Bussmann, J., Witte, M., Chi, N. C., Duckers, H. J. and Schulte-Merker, S. (2009). Ccbe1 is required for embryonic lymphangiogenesis and venous sprouting. *Nat. Genet.* **41**, 396-398.
Hong, K.-J., Hsu, M.-C., Hou, M.-F. and Hung, W.-C. (2011). The tumor suppressor RECK interferes with HER-2/Neu dimerization and attenuates its oncogenic signaling. *FEBS Lett.* **585**, 591-595.
Hong, K.-J., Wu, D.-C., Cheng, K.-H., Chen, L.-T. and Hung, W.-C. (2014). RECK inhibits stemness gene expression and tumorigenicity of gastric cancer cells by suppressing ADAM-mediated Notch1 activation. *J. Cell. Physiol.* **229**, 191-201.
Hu, J., Dong, A., Fernandez-Ruiz, V., Shan, J., Kawa, M., Martinez-Anso, E., Prieto, J. and Qian, C. (2009). Blockade of Wnt signaling inhibits angiogenesis and tumor growth in hepatocellular carcinoma. *Cancer Res.* **69**, 6951-6959.
Imhof, I., Gasper, W. J. and Derynck, R. (2008). Association of tetraspanin CD9 with transmembrane TGF{alpha} confers alterations in cell-surface presentation of TGF{alpha} and cytoskeletal organization. *J. Cell Sci.* **121**, 2265-2274.
Isogai, S., Horiguchi, M. and Weinstein, B. M. (2001). The vascular anatomy of the developing zebrafish: an atlas of embryonic and early larval development. *Dev. Biol.* **230**, 278-301.
Janssens, E., Gaublomme, D., De Groef, L., Darras, V. M., Arckens, L., Delorme, N., Claes, F., Van Hove, I. and Moons, L. (2013). Matrix metalloproteinase 14 in the zebrafish: an eye on retinal and retinotectal development. *PLoS ONE* **8**, e52915.
Kagermeier-Schenk, B., Wehner, D., Ozhan-Kizil, G., Yamamoto, H., Li, J., Kirchner, K., Hoffmann, C., Stern, P., Kikuchi, A., Schambony, A. et al. (2011). Waif1/5T4 inhibits Wnt/beta-catenin signaling and activates noncanonical Wnt pathways by modifying LRP6 subcellular localization. *Dev. Cell* **21**, 1129-1143.
Kaufmann, A., Mickoleit, M., Weber, M. and Huisken, J. (2012). Multilayer mounting enables long-term imaging of zebrafish development in a light sheet microscope. *Development* **139**, 3242-3247.
Klaus, A. and Birchmeier, W. (2008). Wnt signalling and its impact on development and cancer. *Nat. Rev. Cancer* **8**, 387-398.
Klein, P. S. and Melton, D. A. (1996). A molecular mechanism for the effect of lithium on development. *Proc. Natl. Acad. Sci. USA* **93**, 8455-8459.
Koch, S., Tugues, S., Li, X., Gualandi, L. and Claesson-Welsh, L. (2011). Signal transduction by vascular endothelial growth factor receptors. *Biochem. J.* **437**, 169-183.
Kochhan, E., Lenard, A., Ellertsdottir, E., Herwig, L., Affolter, M., Belting, H.-G. and Siekmann, A. F. (2013). Blood flow changes coincide with cellular rearrangements during blood vessel pruning in zebrafish embryos. *PLoS ONE* **8**, e75060.
Kok, F. O., Shin, M., Ni, C.-W., Gupta, A., Grosse, A. S., van Impel, A., Kirchmaier, B. C., Peterson-Maduro, J., Kourkoulis, G., Male, I. et al. (2015). Reverse genetic screening reveals poor correlation between Morpholino-induced and mutant phenotypes in zebrafish. *Dev. Cell* **32**, 97-108.
Kwan, K. M., Fujimoto, E., Grabher, C., Mangum, B. D., Hardy, M. E., Campbell, D. S., Parant, J. M., Yost, H. J., Kanki, J. P. and Chien, C.-B. (2007). The Tol2kit: a multisite gateway-based construction kit for Tol2 transposon transgenesis constructs. *Dev. Dyn.* **236**, 3088-3099.

Lanahan, A., Zhang, X., Fantin, A., Zhuang, Z., Rivera-Molina, F., Speichinger, K., Prahst, C., Zhang, J., Wang, Y., Davis, G. et al. (2013). The neuropilin 1 cytoplasmic domain is required for VEGF-A-dependent arteriogenesis. *Dev. Cell* **25**, 156-168.

Larrivee, B., Prahst, C., Gordon, E., del Toro, R., Mathivet, T., Duarte, A., Simons, M. and Eichmann, A. (2012). ALK1 signaling inhibits angiogenesis by cooperating with the Notch pathway. *Dev. Cell* **22**, 489-500.

Larson, J. D., Wadman, S. A., Chen, E., Kerley, L., Clark, K. J., Eide, M., Lippert, S., Nasevicius, A., Ekker, S. C., Hackett, P. B. et al. (2004). Expression of VE-cadherin in zebrafish embryos: a new tool to evaluate vascular development. *Dev. Dyn.* **231**, 204-213.

Lawson, N. D. and Weinstein, B. M. (2002). In vivo imaging of embryonic vascular development using transgenic zebrafish. *Dev. Biol.* **248**, 307-318.

Lawson, N. D., Vogel, A. M. and Weinstein, B. M. (2002). sonic hedgehog and vascular endothelial growth factor act upstream of the Notch pathway during arterial endothelial differentiation. *Dev. Cell* **3**, 127-136.

Lawson, N. D., Mugford, J. W., Diamond, B. A. and Weinstein, B. M. (2003). phospholipase C gamma-1 is required downstream of vascular endothelial growth factor during arterial development. *Genes Dev.* **17**, 1346-1351.

Liang, D., Chang, J. R., Chin, A. J., Smith, A., Kelly, C., Weinberg, E. S. and Ge, R. (2001). The role of vascular endothelial growth factor (VEGF) in vasculogenesis, angiogenesis, and hematopoiesis in zebrafish development. *Mech. Dev.* **108**, 29-43.

Liebner, S., Corada, M., Bangsow, T., Babbage, J., Taddei, A., Czupalla, C. J., Reis, M., Felici, A., Wolburg, H., Fruttiger, M. et al. (2008). Wnt/beta-catenin signaling controls development of the blood-brain barrier. *J. Cell Biol.* **183**, 409-417.

Lyons, M. S., Bell, B., Stainier, D. and Peters, K. G. (1998). Isolation of the zebrafish homologues for the tie-1 and tie-2 endothelium-specific receptor tyrosine kinases. *Dev. Dyn.* **212**, 133-140.

MacDonald, B. T., Tamai, K. and He, X. (2009). Wnt/beta-catenin signaling: components, mechanisms, and diseases. *Dev. Cell* **17**, 9-26.

Mackenzie, F. and Ruhrberg, C. (2012). Diverse roles for VEGF-A in the nervous system. *Development* **139**, 1371-1380.

Mantuano, E., Inoue, G., Li, X., Takahashi, K., Gaultier, A., Gonias, S. L. and Campana, W. M. (2008). The hemopexin domain of matrix metalloproteinase-9 activates cell signaling and promotes migration of schwann cells by binding to low-density lipoprotein receptor-related protein. *J. Neurosci.* **28**, 11571-11582.

Martin, B. L. and Kimelman, D. (2012). Canonical Wnt signaling dynamically controls multiple stem cell fate decisions during vertebrate body formation. *Dev. Cell* **22**, 223-232.

Masckauchan, T. N. H. and Kitajewski, J. (2006). Wnt/Frizzled signaling in the vasculature: new angiogenic factors in sight. *Physiology* **21**, 181-188.

Mason, A. J. (1994). Functional analysis of the cysteine residues of activin A. *Mol. Endocrinol.* **8**, 325-332.

McGraw, H. F., Nechiporuk, A. and Raible, D. W. (2008). Zebrafish dorsal root ganglia neural precursor cells adopt a glial fate in the absence of neurogenin1. *J. Neurosci.* **28**, 12558-12569.

Meng, X., Noyes, M. B., Zhu, L. J., Lawson, N. D. and Wolfe, S. A. (2008). Targeted gene inactivation in zebrafish using engineered zinc-finger nucleases. *Nat. Biotechnol.* **26**, 695-701.

Mergenthaler, P., Lindauer, U., Dienel, G. A. and Meisel, A. (2013). Sugar for the brain: the role of glucose in physiological and pathological brain function. *Trends Neurosci.* **36**, 587-597.

Miki, T., Shamma, A., Kitajima, S., Takegami, Y., Noda, M., Nakashima, Y., Watanabe, K. I. and Takahashi, C. (2010). The β1-integrin-dependent function of RECK in physiologic and tumor angiogenesis. *Mol. Cancer Res.* **8**, 665-676.

Mori, H., Lo, A. T., Inman, J. L., Alcaraz, J., Ghajar, C. M., Mott, J. D., Nelson, C. M., Chen, C. S., Zhang, H., Bascom, J. L. et al. (2013). Transmembrane/cytoplasmic, rather than catalytic, domains of Mmp14 signal to MAPK activation and mammary branching morphogenesis via binding to integrin beta1. *Development* **140**, 343-352.

Moro, E., Vettori, A., Porazzi, P., Schiavone, M., Rampazzo, E., Casari, A., Ek, O., Facchinello, N., Astone, M., Zancan, I. et al. (2013). Generation and application of signaling pathway reporter lines in zebrafish. *Mol. Genet. Genom.* **288**, 231-242.

Muraguchi, T., Takegami, Y., Ohtsuka, T., Kitajima, S., Chandana, E. P. S., Omura, A., Miki, T., Takahashi, R., Matsumoto, N., Ludwig, A. et al. (2007). RECK modulates Notch signaling during cortical neurogenesis by regulating ADAM10 activity. *Nat. Neurosci.* **10**, 838-845.

Nagini, S. (2012). RECKing MMP: relevance of reversion-inducing cysteine-rich protein with kazal motifs as a prognostic marker and therapeutic target for cancer (a review). *Anti-cancer Agents Med. Chem.* **12**, 718-725.

Nicoli, S., Standley, C., Walker, P., Hurlstone, A., Fogarty, K. E. and Lawson, N. D. (2010). MicroRNA-mediated integration of haemodynamics and Vegf signalling during angiogenesis. *Nature* **464**, 1196-1200.

Noda, M. and Takahashi, C. (2007). Recklessness as a hallmark of aggressive cancer. *Cancer Sci.* **98**, 1659-1665.

Obermeier, B., Daneman, R. and Ransohoff, R. M. (2013). Development, maintenance and disruption of the blood-brain barrier. *Nat. Med.* **19**, 1584-1596.

Oh, J., Takahashi, R., Kondo, S., Mizoguchi, A., Adachi, E., Sasahara, R. M., Nishimura, S., Imamura, Y., Kitayama, H., Alexander, D. B. et al. (2001). The membrane-anchored MMP inhibitor RECK is a key regulator of extracellular matrix integrity and angiogenesis. *Cell* **107**, 789-800.

Olszewska-Pazdrak, B., Hein, T. W., Olszewska, P. and Carney, D. H. (2009). Chronic hypoxia attenuates VEGF signaling and angiogenic responses by downregulation of KDR in human endothelial cells. *Am. J. Physiol. Cell Physiol.* **296**, C1162-C1170.

Omura, A., Matsuzaki, T., Mio, K., Ogura, T., Yamamoto, M., Fujita, A., Okawa, K., Kitayama, H., Takahashi, C., Sato, C. et al. (2009). RECK forms cowbell-shaped dimers and inhibits matrix metalloproteinase-catalyzed cleavage of fibronectin. *J. Biol. Chem.* **284**, 3461-3469.

Ousman, S. S. and Kubes, P. (2012). Immune surveillance in the central nervous system. *Nat. Neurosci.* **15**, 1096-1101.

Page-McCaw, A., Ewald, A. J. and Werb, Z. (2007). Matrix metalloproteinases and the regulation of tissue remodelling. *Nat. Rev. Mol. Cell Biol.* **8**, 221-233.

Park, S., Lee, C., Sabharwal, P., Zhang, M., Meyers, C. L. F. and Sockanathan, S. (2013). GDE2 promotes neurogenesis by glycosylphosphatidylinositol-anchor cleavage of RECK. *Science* **339**, 324-328.

Posokhova, E., Shukla, A., Seaman, S., Volate, S., Hilton, M. B., Wu, B., Morris, H., Swing, D. A., Zhou, M., Zudaire, E. et al. (2015). GPR124 functions as a WNT7-specific coactivator of canonical beta-catenin signaling. *Cell Rep.* **10**, 123-130.

Prendergast, A., Linbo, T. H., Swarts, T., Ungos, J. M., McGraw, H. F., Krispin, S., Weinstein, B. M. and Raible, D. W. (2012). The metalloproteinase inhibitor Reck is essential for zebrafish DRG development. *Development* **139**, 1141-1152.

Prieve, M. G. and Waterman, M. L. (1999). Nuclear localization and formation of beta-catenin-lymphoid enhancer factor 1 complexes are not sufficient for activation of gene expression. *Mol. Cell. Biol.* **19**, 4503-4515.

Qian, F., Zhen, F., Ong, C., Jin, S.-W., Meng Soo, H., Stainier, D. Y. R., Lin, S., Peng, J. and Wen, Z. (2005). Microarray analysis of zebrafish cloche mutant using amplified cDNA and identification of potential downstream target genes. *Dev. Dyn.* **233**, 1163-1172.

Rahmah, N. N., Sakai, K., Sano, K. and Hongo, K. (2012). Expression of RECK in endothelial cells of glioma: comparison with CD34 and VEGF expressions. *J. Neuro-Oncol.* **107**, 559-564.

Reis, M. and Liebner, S. (2013). Wnt signaling in the vasculature. *Exp. Cell Res.* **319**, 1317-1323.

Rims, C. R. and McGuire, J. K. (2014). Matrilysin (MMP-7) catalytic activity regulates beta-catenin localization and signaling activation in lung epithelial cells. *Exp. Lung Res.* **40**, 126-136.

Ring, D. B., Johnson, K. W., Henriksen, E. J., Nuss, J. M., Goff, D., Kinnick, T. R., Ma, S. T., Reeder, J. W., Samuels, I., Slabiak, T. et al. (2003). Selective glycogen synthase kinase 3 inhibitors potentiate insulin activation of glucose transport and utilization in vitro and in vivo. *Diabetes* **52**, 588-595.

Rolfe, D. F. and Brown, G. C. (1997). Cellular energy utilization and molecular origin of standard metabolic rate in mammals. *Physiol. Rev.* **77**, 731-758.

Ruhrberg, C. and Bautch, V. L. (2013). Neurovascular development and links to disease. *Cell. Mol. Life Sci.* **70**, 1675-1684.

Sakao, S. and Tatsumi, K. (2011). The effects of antiangiogenic compound SU5416 in a rat model of pulmonary arterial hypertension. *Respiration* **81**, 253-261.

Schrijver, I., Liu, W., Brenn, T., Furthmayr, H. and Francke, U. (1999). Cysteine substitutions in epidermal growth factor-like domains of fibrillin-1: distinct effects on biochemical and clinical phenotypes. *Am. J. Hum. Genet.* **65**, 1007-1020.

Schulte-Merker, S. and Stainier, D. Y. R. (2014). Out with the old, in with the new: reassessing morpholino knockdowns in light of genome editing technology. *Development* **141**, 3103-3104.

Seals, D. F. and Courtneidge, S. A. (2003). The ADAMs family of metalloproteases: multidomain proteins with multiple functions. *Genes Dev.* **17**, 7-30.

Sehnert, A. J., Huq, A., Weinstein, B. M., Walker, C., Fishman, M. and Stainier, D. Y. R. (2002). Cardiac troponin T is essential in sarcomere assembly and cardiac contractility. *Nat. Genet.* **31**, 106-110.

Shaw, K. M., Castranova, D. A., Pham, V. N., Kamei, M., Kidd, K. R., Lo, B. D., Torres-Vasquez, J., Ruby, A. and Weinstein, B. M. (2006). fused-somites-like mutants exhibit defects in trunk vessel patterning. *Dev. Dyn.* **235**, 1753-1760.

Siegenthaler, J. A., Sohet, F. and Daneman, R. (2013). 'Sealing off the CNS': cellular and molecular regulation of blood-brain barriergenesis. *Curr. Opin. Neurobiol.* **23**, 1057-1064.

Silveira Correa, T. C., Massaro, R. R., Brohem, C. A., Taboga, S. R., Lamers, M. L., Santos, M. F. and Maria-Engler, S. S. (2010). RECK-mediated inhibition of glioma migration and invasion. *J. Cell. Biochem.* **110**, 52-61.

Simizu, S., Takagi, S., Tamura, Y. and Osada, H. (2005). RECK-mediated suppression of tumor cell invasion is regulated by glycosylation in human tumor cell lines. *Cancer Res.* **65**, 7455-7461.

Sivaraj, K. K., Takefuji, M., Schmidt, I., Adams, R. H., Offermanns, S. and Wettschureck, N. (2013). G13 controls angiogenesis through regulation of VEGFR-2 expression. *Dev. Cell* **25**, 427-434.

Snow, C. J., Peterson, M. T., Khalil, A. and Henry, C. A. (2008). Muscle development is disrupted in zebrafish embryos deficient for fibronectin. *Dev. Dyn.* **237**, 2542-2553.
Sohet, F. and Daneman, R. (2013). Genetic mouse models to study blood-brain barrier development and function. *Fluids Barriers CNS* **10**, 3.
Srivastava, A., Pastor-Pareja, J. C., Igaki, T., Pagliarini, R. and Xu, T. (2007). Basement membrane remodeling is essential for Drosophila disc eversion and tumor invasion. *Proc. Natl. Acad. Sci. USA* **104**, 2721-2726.
Stainier, D. Y. R., Kontarakis, Z. and Rossi, A. (2015). Making sense of anti-sense data. *Dev. Cell* **32**, 7-8.
Stamos, J. L. and Weis, W. I. (2013). The beta-catenin destruction complex. *Cold Spring Harb. Perspect. Biol.* **5**, a007898.
Stenman, J. M., Rajagopal, J., Carroll, T. J., Ishibashi, M., McMahon, J. and McMahon, A. P. (2008). Canonical Wnt signaling regulates organ-specific assembly and differentiation of CNS vasculature. *Science* **322**, 1247-1250.
Taelman, V. F., Dobrowolski, R., Plouhinec, J.-L., Fuentealba, L. C., Vorwald, P. P., Gumper, I., Sabatini, D. D. and De Robertis, E. M. (2010). Wnt signaling requires sequestration of glycogen synthase kinase 3 inside multivesicular endosomes. *Cell* **143**, 1136-1148.
Takahashi, C., Sheng, Z., Horan, T. P., Kitayama, H., Maki, M., Hitomi, K., Kitaura, Y., Takai, S., Sasahara, R. M., Horimoto, A. et al. (1998). Regulation of matrix metalloproteinase-9 and inhibition of tumor invasion by the membrane-anchored glycoprotein RECK. *Proc. Natl. Acad. Sci. USA* **95**, 13221-13226.
Tam, S. J., Richmond, D. L., Kaminker, J. S., Modrusan, Z., Martin-McNulty, B., Cao, T. C., Weimer, R. M., Carano, R. A. D., van Bruggen, N. and Watts, R. J. (2012). Death receptors DR6 and TROY regulate brain vascular development. *Dev. Cell* **22**, 403-417.
Traver, D., Paw, B. H., Poss, K. D., Penberthy, W. T., Lin, S. and Zon, L. I. (2003). Transplantation and in vivo imaging of multilineage engraftment in zebrafish bloodless mutants. *Nat. Immunol.* **4**, 1238-1246.
Ulrich, F., Ma, L.-H., Baker, R. G. and Torres-Vazquez, J. (2011). Neurovascular development in the embryonic zebrafish hindbrain. *Dev. Biol.* **357**, 134-151.
Umans, R. A. and Taylor, M. R. (2012). Zebrafish as a model to study drug transporters at the blood-brain barrier. *Clin. Pharmacol. Ther.* **92**, 567-570.
Vallon, M., Chang, J., Zhang, H. and Kuo, C. J. (2014). Developmental and pathological angiogenesis in the central nervous system. *Cell. Mol. Life Sci.* **71**, 3489-3506.
Vanhollebeke, B., Stone, O. A., Bostaille, N., Cho, C., Zhou, Y., Maquet, E., Gauquier, A., Cabochette, P., Fukuhara, S., Mochizuki, N. et al. (2015). Tip cell-specific requirement for an atypical Gpr124- and Reck-dependent Wnt/beta-catenin pathway during brain angiogenesis. *Elife* **4**, e06489.
Veldman, M. B., Zhao, C., Gomez, G. A., Lindgren, A. G., Huang, H., Yang, H., Yao, S., Martin, B. L., Kimelman, D. and Lin, S. (2013). Transdifferentiation of fast skeletal muscle into functional endothelium in vivo by transcription factor Etv2. *PLoS Biol.* **11**, e1001590.
Venkiteswaran, G., Lewellis, S. W., Wang, J., Reynolds, E., Nicholson, C. and Knaut, H. (2013). Generation and dynamics of an endogenous, self-generated signaling gradient across a migrating tissue. *Cell* **155**, 674-687.
Villefranc, J. A., Amigo, J. and Lawson, N. D. (2007). Gateway compatible vectors for analysis of gene function in the zebrafish. *Dev. Dyn.* **236**, 3077-3087.
Wada, H., Ghysen, A., Asakawa, K., Abe, G., Ishitani, T. and Kawakami, K. (2013). Wnt/Dkk negative feedback regulates sensory organ size in zebrafish. *Curr. Biol.* **23**, 1559-1565.
Wang, Y. and Nakayama, N. (2009). WNT and BMP signaling are both required for hematopoietic cell development from human ES cells. *Stem Cell Res.* **3**, 113-125.
Wang, Y., Cho, S.-G., Wu, X., Siwko, S. and Liu, M. (2014). G-protein coupled receptor 124 (GPR124) in endothelial cells regulates vascular endothelial growth factor (VEGF)-induced tumor angiogenesis. *Curr. Mol. Med.* **14**, 543-554.
Watson, O., Novodvorsky, P., Gray, C., Rothman, A. M. K., Lawrie, A., Crossman, D. C., Haase, A., McMahon, K., Gering, M., Van Eeden, F. J. M. et al. (2013). Blood flow suppresses vascular Notch signalling via dll4 and is required for angiogenesis in response to hypoxic signalling. *Cardiovasc. Res.* **100**, 252-261.
Wittko-Schneider, I. M., Schneider, F. T. and Plate, K. H. (2013). Brain homeostasis: VEGF receptor 1 and 2-two unequal brothers in mind. *Cell. Mol. Life Sci.* **70**, 1705-1725.
Wu, S.-Y., Shin, J., Sepich, D. S. and Solnica-Krezel, L. (2012). Chemokine GPCR signaling inhibits beta-catenin during zebrafish axis formation. *PLoS Biol.* **10**, e1001403.
Wythe, J. D., Dang, L. T. H., Devine, W. P., Boudreau, E., Artap, S. T., He, D., Schachterle, W., Stainier, D. Y. R., Oettgen, P., Black, B. L. et al. (2013). ETS factors regulate VEGF-dependent arterial specification. *Dev. Cell* **26**, 45-58.
Yamamoto, M., Matsuzaki, T., Takahashi, R., Adachi, E., Maeda, Y., Yamaguchi, S., Kitayama, H., Echizenya, M., Morioka, Y., Alexander, D. B. et al. (2012). The transformation suppressor gene Reck is required for postaxial patterning in mouse forelimbs. *Biol. Open* **1**, 458-466.
Yost, C., Torres, M., Miller, J. R., Huang, E., Kimelman, D. and Moon, R. T. (1996). The axis-inducing activity, stability, and subcellular distribution of beta-catenin is regulated in Xenopus embryos by glycogen synthase kinase 3. *Genes Dev.* **10**, 1443-1454.
Zachary, I. (2003). VEGF signalling: integration and multi-tasking in endothelial cell biology. *Biochem. Soc. Trans.* **31**, 1171-1177.
Zhou, Y. and Nathans, J. (2014). Gpr124 controls CNS angiogenesis and blood-brain barrier integrity by promoting ligand-specific canonical wnt signaling. *Dev. Cell* **31**, 248-256.
Zhou, Y., Wang, Y., Tischfield, M., Williams, J., Smallwood, P. M., Rattner, A., Taketo, M. M. and Nathans, J. (2014). Canonical WNT signaling components in vascular development and barrier formation. *J. Clin. Invest.* **124**, 3825-3846.
Zygmunt, T., Gay, C. M., Blondelle, J., Singh, M. K., Flaherty, K. M., Means, P. C., Herwig, L., Krudewig, A., Belting, H.-G., Affolter, M. et al. (2011). Semaphorin-PlexinD1 signaling limits angiogenic potential via the VEGF decoy receptor sFlt1. *Dev. Cell* **21**, 301-314.

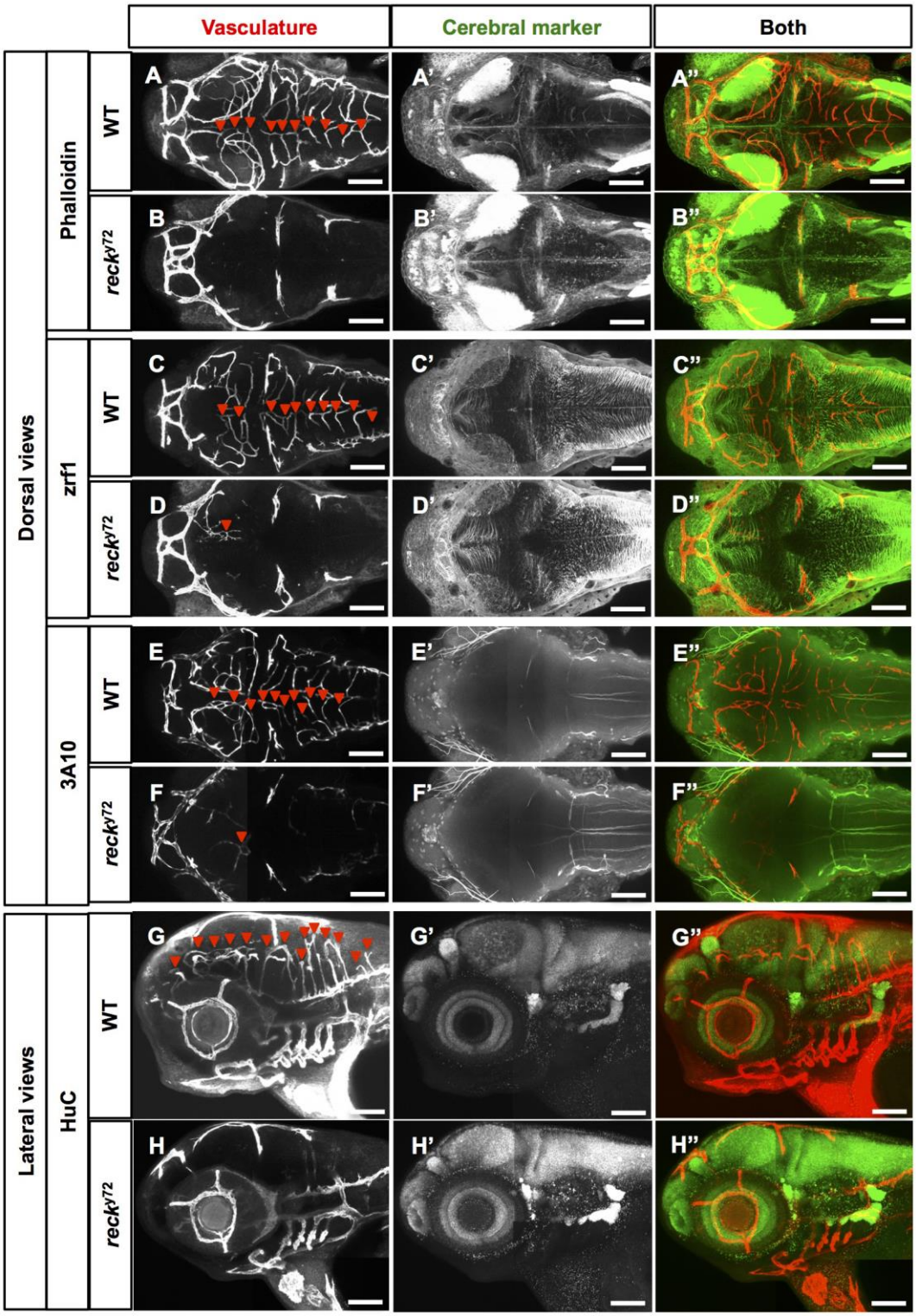

Fig. S1. Normal gross cerebral organization in *reck*^{y72}. (A-H'') Confocal views; 72 hpf embryo heads. Anterior, left. (A-F"') Dorsal views; left side, bottom. (G-H") Lateral views; dorsal, up. Scale Bar: 100 µm. Genotypes, vasculature and cerebral markers as indicated. Vasculature: *Tg(kdrl:RFP)*^{s896} or *Tg(kdrl:eGFP)*^{1a116}. Cerebral markers: phalloidin staining (labels F-actin at the interface of actin subunits), zrf1 (radial glia), 3A10 (labels a subset of hindbrain spinal cord projecting neurons, including Mauthner neurons) and HuC (pan-neuronal marker) immunofluorescence; see (Brand et al., 1996; Kim et al., 1996; Lowery et al., 2009)(Ulrich et al., 2011).

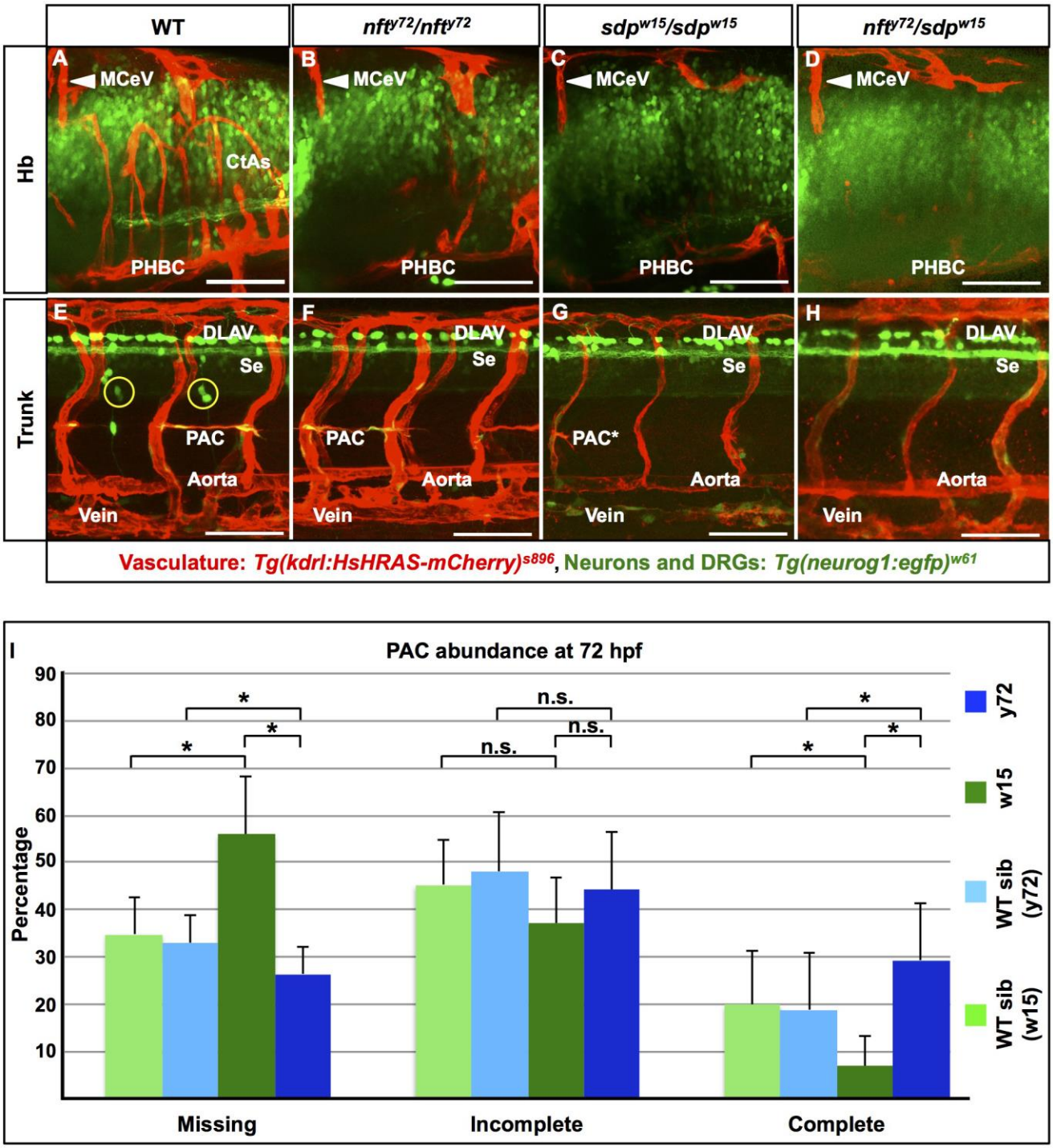

Fig. S2. *nft*^{y72}/*sdp*^{w15} trans-heterozygotes and both *nft*^{y72} and *sdp*^{w15} homozygotes have identical CtA and DRG deficits. (A-H) Confocal lateral images of the Hb (A-D) and trunk (E-H) of 72 hpf embryos. Anterior, left; dorsal, up. Vasculature (white labels), red (*Tg(kdrl:RFP)*^{s896}); DRG neurons, green (in yellow circles, *Tg(neurog1:eGFP)*^{w61}). Scale bars: 100 µm. (I) Quantification of the abundance of missing, incomplete and complete Parachordal Chains (PAC) at 72 hpf in *nft*^{y72} (*reck*^{y72}) and *sdp*^{w15} (*Df(Chr24:reck)*^{w15}) mutants and their phenotypically-WT siblings. A complete PAC spans the full distance between an ipsilateral Se vessel pair. PAC percentages were thus calculated in reference to the total number of Se vessel pairs scored. Asterisks, significant differences ($p < 0.05$) between genotypes (Student's *t*-test); n.s., no significant. n=10 embryos per genotype or phenotype.

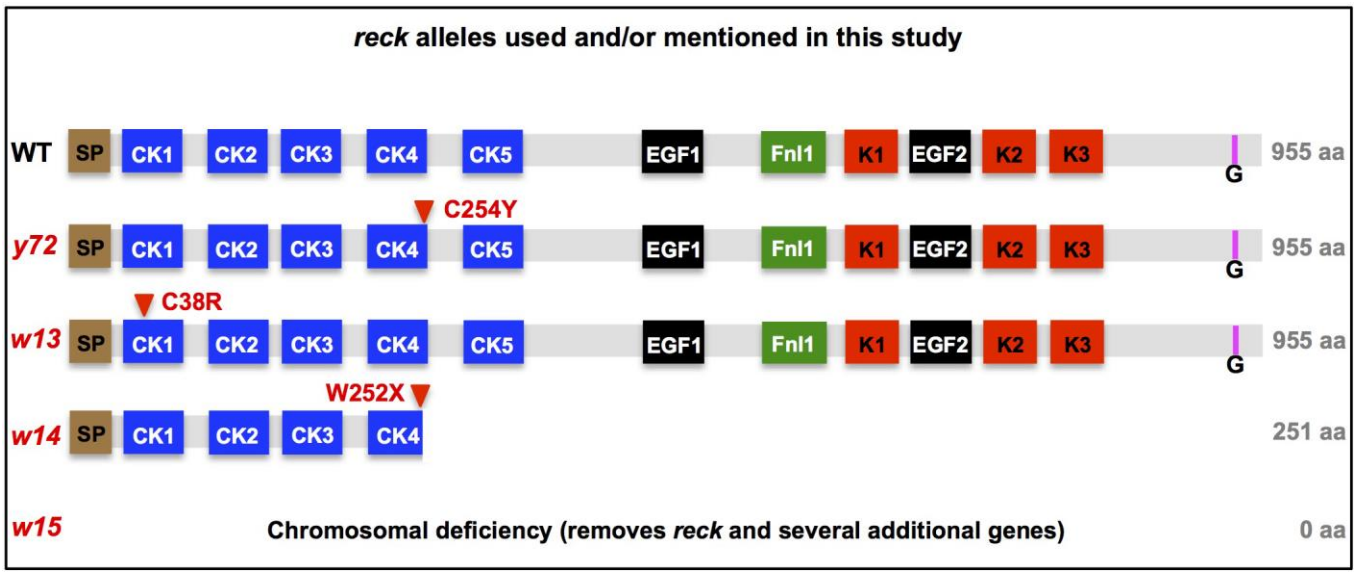

Fig. S3. Domains and sizes of Reck proteins (based on conceptual translation) encoded by the mutant alleles used and/or mentioned in this study. See Table S1.

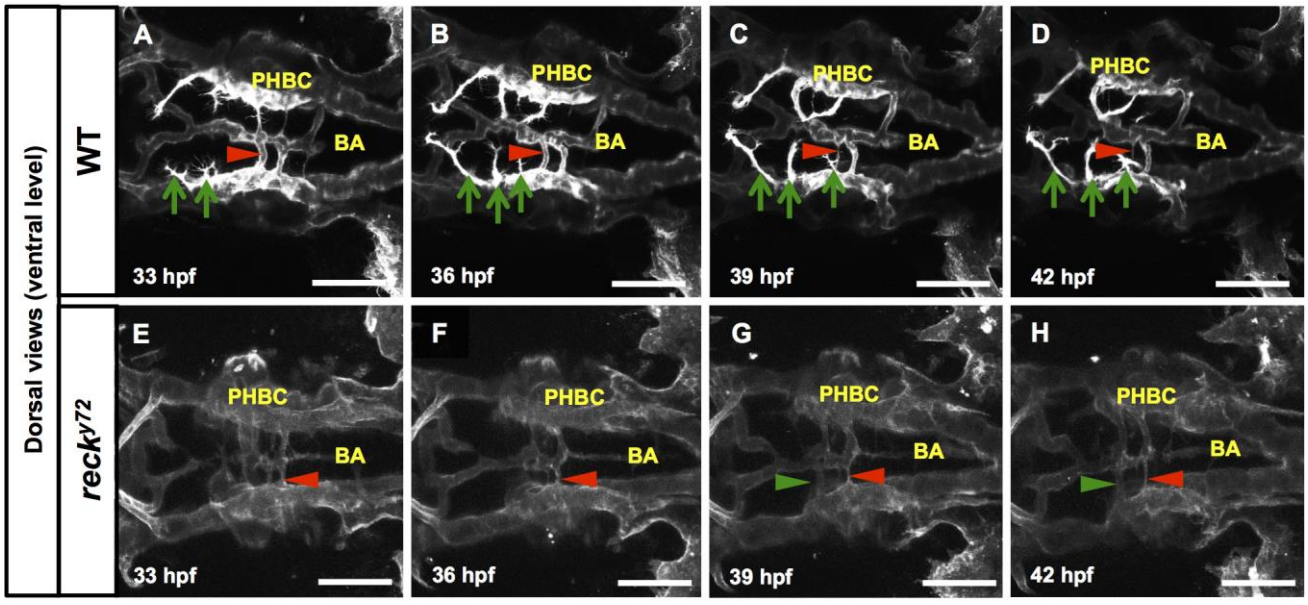

Fig. S4. In *reck*^{y72} the PHBCs are deficient in CtA sprout formation and display abnormal avc dynamics. Time-lapse stills (dorsal views, ventral-level) of Hb vascular development (visualized with *Tg(kdrl:GFP)*^{la116}) in WT (A-D) and *reck*^{y72} (E-H) from 33 to 42 hpf. Anterior, left; right side, up. Green arrows, developing CtA sprouts on the embryo's left side. Green arrows, *de novo* avc formation. Red arrowheads, regressing avc. In this WT (A-D) three filopodia-rich CtA sprouts launch from the dorsal side of the left PHBC, one PHBC-BA avc thins and regresses but no new avc develop. In this *reck*^{y72} (E-H) filopodial activity is absent from the dorsal face of the PHBCs and, accordingly, no CtA-like, dorsally projecting sprouts emerge. On the mutant's left side a PHBC-BA avc regresses and another forms. There is no evidence that the mutant's supernumerary avc are mistargeted CtAs unable to invade the brain. Scale bars: 100 µm. See Movies S2A-S2B.

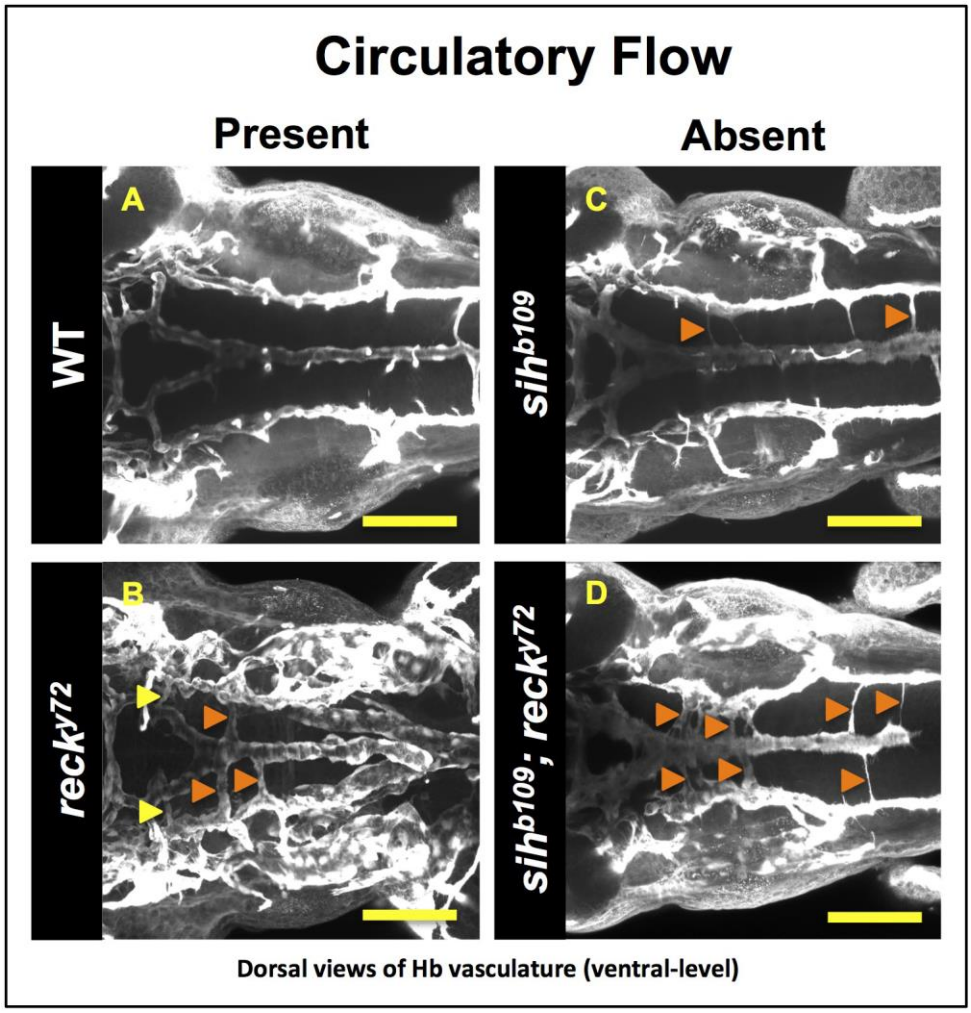

Fig. S5. *reck* limits avc abundance even in the absence of circulatory flow. (A-D) Confocal images (dorsal view) of the 48 hpf peri-neural vasculature. Genotypes as indicated. Arrowheads, avc (PCS-connected, yellow; BA-connected, orange). Scale bars: 100 µm. See Table S2.

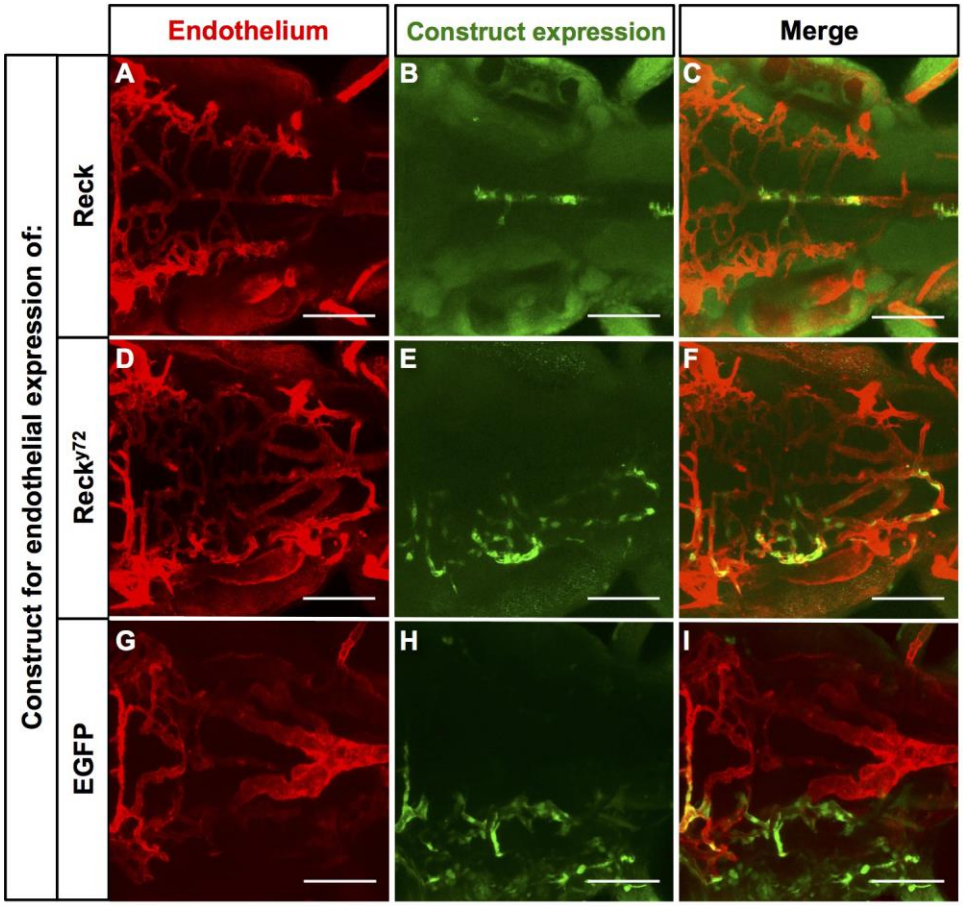

Fig. S6. Examples of the distribution of clones with exogenous endothelial expression of Reck, Reck^{y72} or EGFP in the 72 hpf Hb vasculature of *reck*^{y72} mutants. (A-I) Dorsal views (ventral-level) of the Hb extra-cerebral vasculature (red, *Tg(kdrl:RFP)*^{s896}) of *reck*^{y72} injected with constructs driving endothelial expression of exogenous Reck, Reck^{y72} (both HA-tagged, see Fig. 2L) or EGFP proteins (green). Anterior, left. Right side, up. Scale Bars: 100 µm. See also Figure 5 and Graph S1.

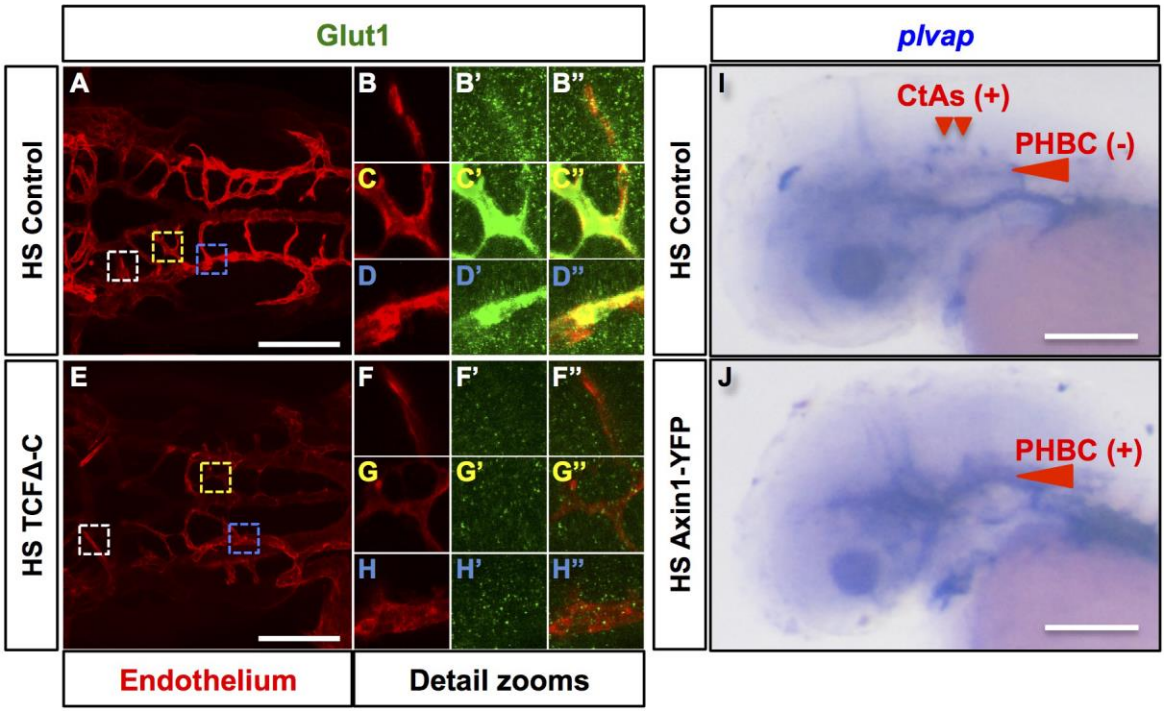

Fig. S7. Forced inhibition of canonical Wnt signaling impairs CtA formation and leads to aberrant cerebrovascular expression of the Wnt-responsive markers of barriergenic differentiation Glut1 and *plvap*. (A-H") Confocal dorsal images of the 48 hpf Hb vasculatures of heat-shocked (HS) embryos without (Control) or with TCFΔC (*Tg(hsp70l:Xla.TCFΔC-EGFP*) over-expression. Heat-shock: 40ºC for 30 minutes at 30 hpf. Anterior, left. Right side, up. Endothelium, red (*Tg(kdrl:RFP)*^{s896}); Glut1 immunofluorescence, green. Colored dashed boxes (A, E) demarcate a region of the following vessels: white, MtA (zooms: B-B", F-F"); yellow, CtAs (zooms: C-C", G-G"); blue, PHBCs (zooms: D-D", H-H"). Merged images of zooms: B", C", D", F", G", H". Glut1 decorates the MtA, CtAs and PHBCs of the Control (n=2 embryos). In contrast, in the TCFΔC over-expressing embryo CtA abundance is reduced (n=10 embryos) and cerebrovascular Glut1 decoration is missing (n=2 embryos). (I-J) Transmitted-light lateral images of the 48 hpf heads of heat-shocked (HS) embryos without (Control) or with Axin1-YFP (*Tg(hsp70l:Mmu.Axin1-YFP)*^{w35}) over-expression subjected to whole mount RNA *in situ* hybridization with *plvap* riboprobes. Heat-shock: 39ºC for 1 hour at 24 hpf. (I) Control. *plvap* is expressed in the dorsal aspect of CtAs but not in the PHBCs (n=9 embryos). (J) Axin1-YFP over-expressing embryo. *plvap* is ectopically expressed in the PHBCs (n=7 embryos). Anterior left. Dorsal up. Scale bar: 100 μm.

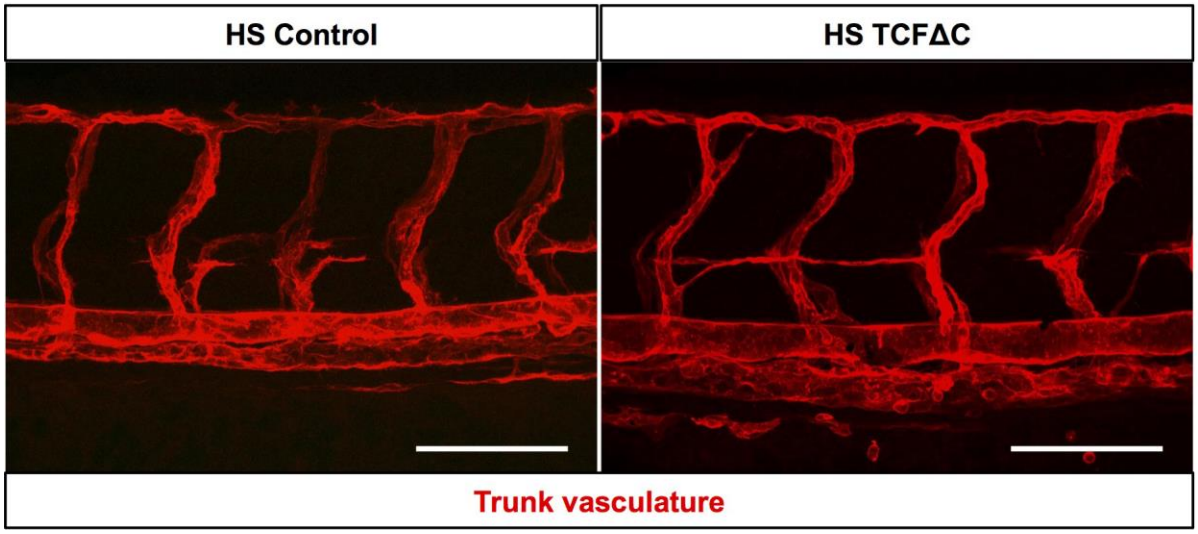

Fig. S8. Forced inhibition of canonical Wnt signaling at 30 hpf has no impact on the patterning of the trunk vasculature. Confocal lateral images of the 48 hpf trunk vasculatures (red; *Tg(kdrl:RFP)*^{s896}) of heat-shocked (HS) embryos without (Control) or with TCFΔC (*Tg(hsp70l:Xla.TCFΔC-EGFP)* over-expression. Heat-shock: 40ºC for 30 minutes at 30 hpf. Anterior, left; dorsal, up. Scale bars: 100 µm.

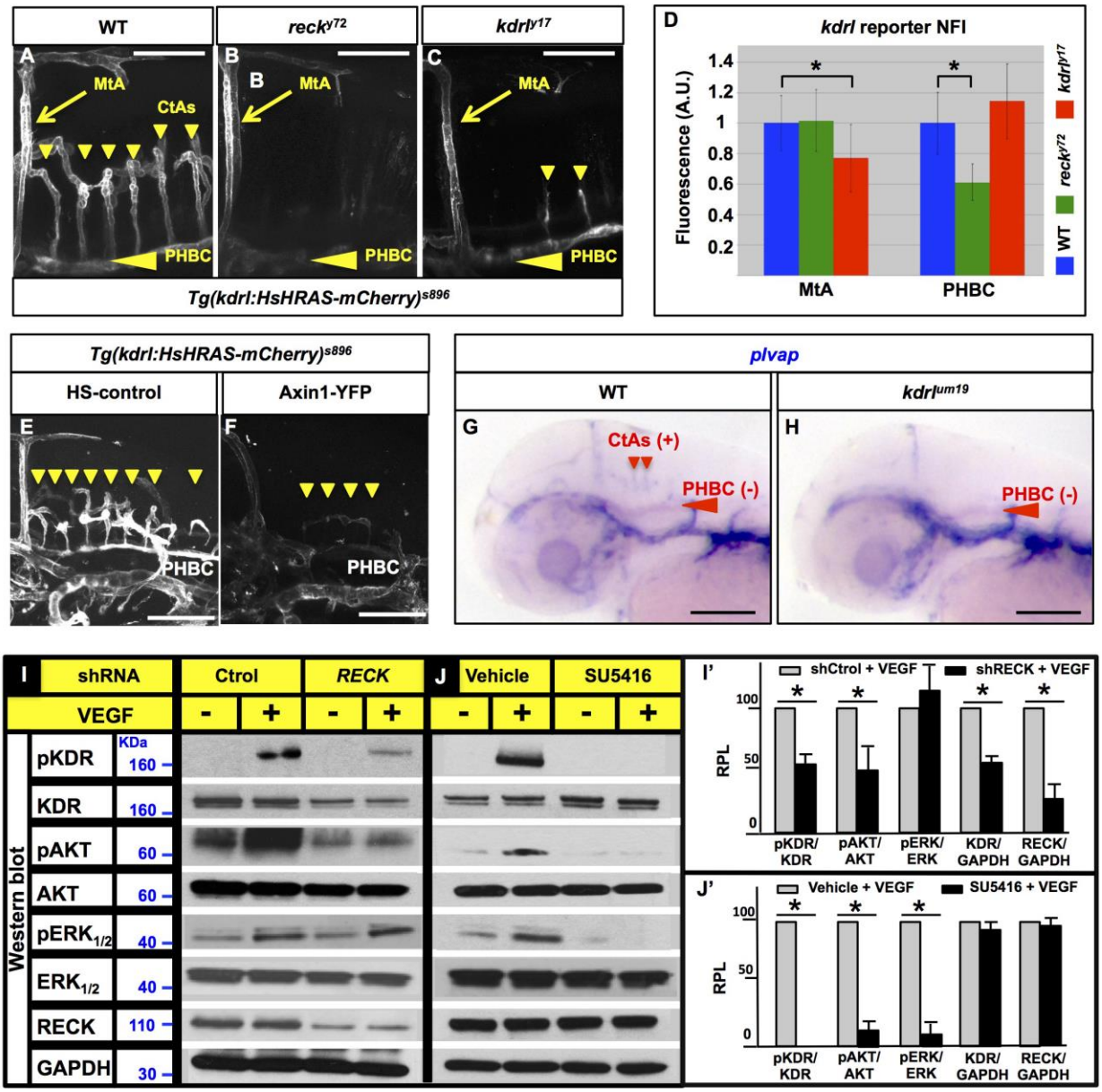

Fig. S9. *reck* and canonical Wnt signaling promote the cerebrovascular expression of the transgenic *kdrl* transcriptional reporter *Tg(kdrl:RFP)*^{s896} in zebrafish and *RECK* promotes VEGF signaling in HUVEC. (A-C, E-F) Confocal lateral images of the live fluorescence of *Tg(kdrl:RFP)*^{s896} (white) in the Hb vasculatures of WT (A), *reck*^{y72} (B), *kdrl*^{y17} (C) and heat-shocked (HS) embryos without (E) or with (F) inhibition of canonical Wnt signaling via Axin1-YFP (*Tg(hsp70l:Mmu.Axin1-YFP)*^{w35}) over-expression. Anterior, left; dorsal, up. (A-C) 58 hpf. (E-F) 48 hpf. (D) Quantification of the Normalized Fluorescence Intensity (NFI) of *Tg(kdrl:RFP)*^{s896} in the MtAs and PHBCs of WT, *reck*^{y72} and *kdrl*^{y17} at 58 hpf expressed in fluorescence Arbitrary Units (A. U.). Asterisks, significant differences (p<0.05). Student's t-test. n=10 embryos per genotype. Vertical lines, SD. (A-D) The PHBC fluorescence of *Tg(kdrl:RFP)*^{s896} is reduced in *reck*^{y72} but not in *kdrl*^{y17}, while that of the MtA is only reduced in *kdrl*^{y17}. (E-F) Both CtA abundance and *Tg(kdrl:RFP)*^{s896} cerebrovascular fluorescence are reduced in Axin1-YFP over-expressing 48 hpf embryos. Heat-shock: 39°C for 1 hour at 24 hpf. (G-H) Transmitted-light lateral images of the 48 hpf heads of phenotypically WT-siblings (G) and *kdrl*^{um19} (H) subjected to whole mount RNA *in situ* hybridization with *plvap* riboprobes. In the WT siblings *plvap* is expressed (+) in the dorsal aspect of CtAs but not (-) in the PHBCs (n=11 embryos). In *kdrl*^{um19} mutants *plvap* is also not expressed (-) in the PHBCs (n=11 embryos) and the CtAs are missing. (A-C, E-H) Small down-pointing arrowheads (yellow or red), CtAs; large left-pointing arrowheads (yellow or red), PHBCs. Scale bars: 100 µm. (I, J) Western Blots of biochemical readouts of VEGF-A signaling. Conditions, above. Detected proteins and molecular weight markers, left. (I', J') Bar graphs of Western Blot quantifications. y axis, Relative Protein Level (RPL) measured by densitometry. x axis, protein and/or phospho-isoform. n=3. Asterisks, significant differences (p<0.05); Student's t-test (vertical lines, SEM).

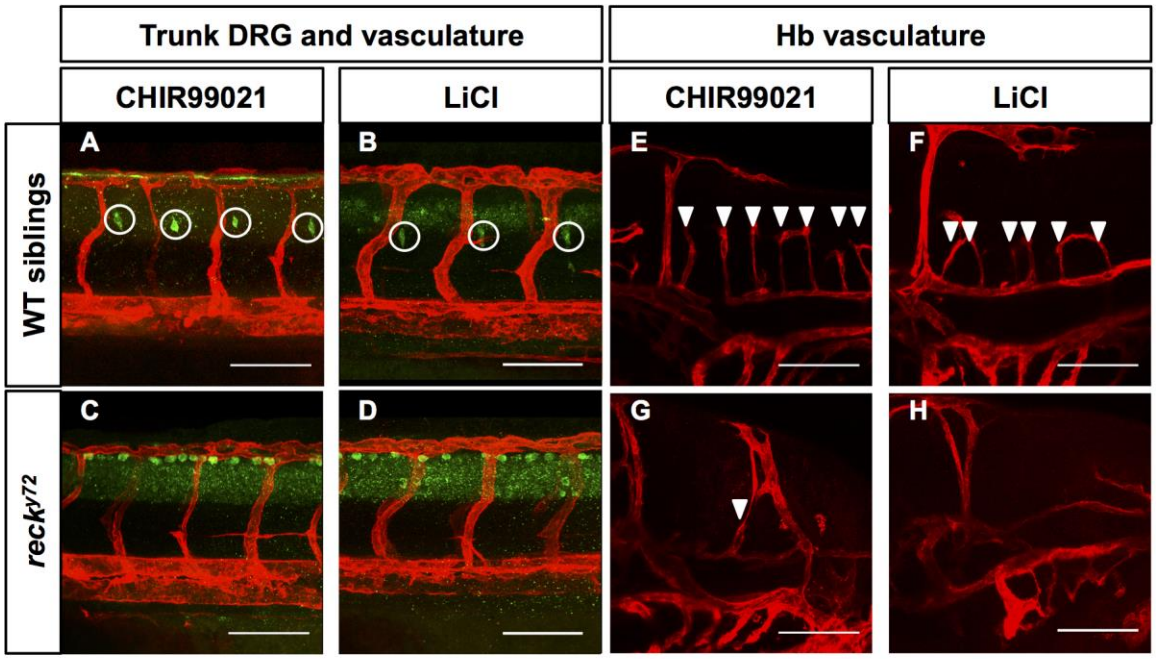

I	DRG abundance (%)		
Genotype	DMSO	CHIR99021	LiCl
WT	21/21 = 100% n = 8 embryos	14/14 = 100% n = 4 embryos	25/27 = 92.6% n = 8 embryos
reck^{y72}	0/19 = 0% n = 5 embryos	0/37 = 0% n = 10 embryos	0/34 = 0% n = 10 embryos

Fig. S10. Chemical activation of canonical Wnt signaling with the GSK3β inhibitors CHIR99021 and LiCl fails to rescue the DRG and CtA deficits of *reck*^{y72} mutants. (A-H) Confocal lateral images at 72 hpf. Anterior, left; dorsal, up. Scale Bars: 100 µm. Genotypes and treatments as indicated. (A-D) DRG (white circles, green HuC immunofluorescence) and vasculature (*Tg(kdrl:HsHRAS-mCherry)*^{s896}; red) in the trunk. (E-H) Hb vasculature (*Tg(kdrl:HsHRAS-mCherry)*^{s896}; red). Central Arteries (CtA; white arrowheads). (I) Quantification of DRG abundance in WT and *reck*^{y72} mutants treated with DMSO vehicle, CHIR99021 and LiCl. DRG abundance was scored by imaging a region of the anterior trunk at the level of the yolk extension spanning 3-4 Se vessels (in WT animals there is one DRG per Se vessel). Thus, the percentages were calculated from the ratio of DRG found/DRG expected.

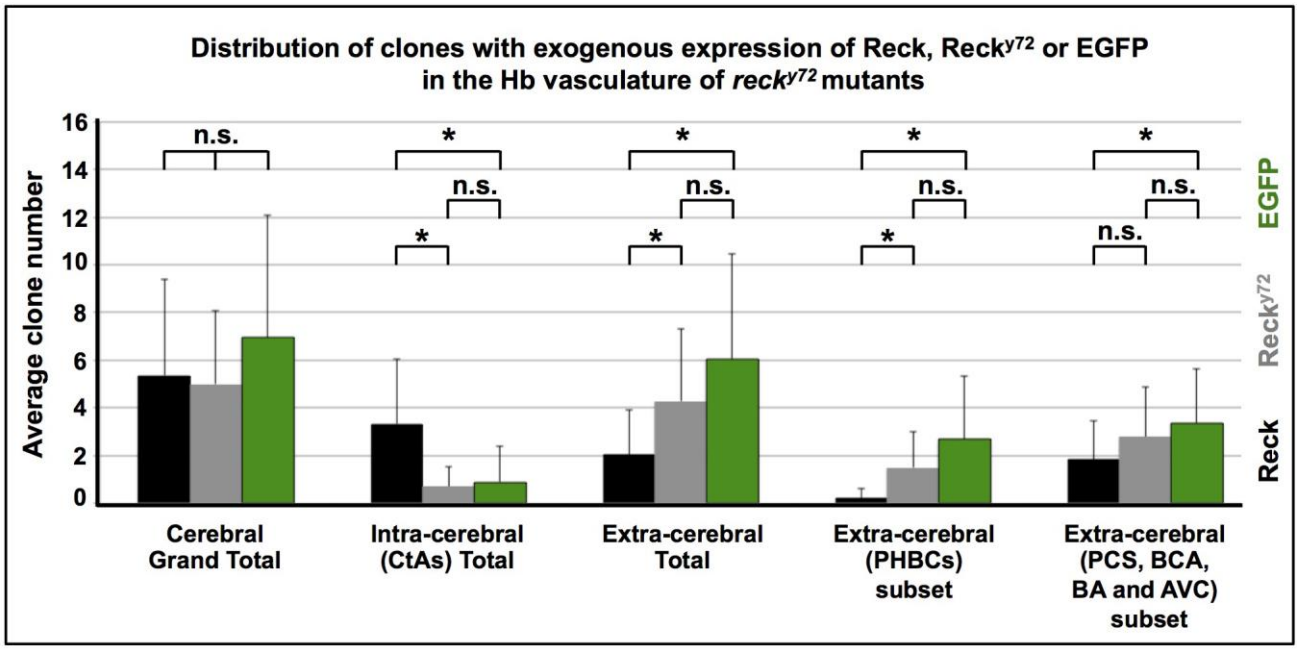

Fig. S11. Similar abundance but differential distribution of clones with exogenous endothelial expression of Reck, Reck^{y72} or EGFP in the 72 hpf Hb vasculature of *reck^{y72}* mutants. Reck-expressing clones are over-represented in the intra-cerebral vessels but under-represented in extra-cerebral vessels (particularly in the PHBCs). Conversely, Reck^{y72}- and EGFP-expressing clones are under-represented in the intra-cerebral vessels but over-represented in the extra-cerebral vessels. Together, these observations indicate that mosaic endothelial expression of Reck is sufficient to enable PHBC cells to emigrate to form CtAs, consistent with the results of our cell transplantation experiments; see Fig. 4G. Asterisks, significant differences (p<0.05); n.s., not significant. Student's t-test (vertical lines, S. E. M.). *reck^{y72}* mutants scored: Reck (n=28), Reck^{y72} (n=14), EGFP (n=19). Both Reck and Reck^{y72} are HA-tagged. See also Figs. 2L, 5.

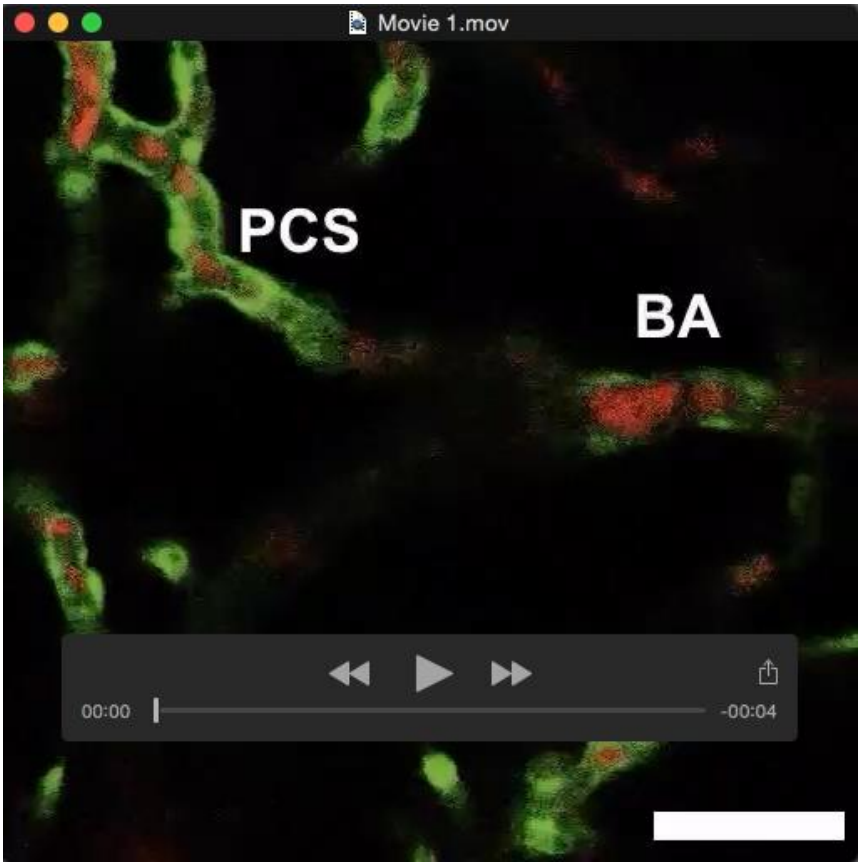

Movie 1. Dorsal view of blood flow through the anterior extra-cerebral Hb vasculature (WT, 2 dpf). Representative confocal time-lapse movie (10 frames/s); single plane. Anterior, left. Left side, bottom. Endothelium, green (*Tg(kdrl:EGFP)*^{la116}); erythrocytes, red (*Tg(gata1a:DsRed)*^{sd2}). Blood flows through the PCS and BA. Scale bar: 85 µm.

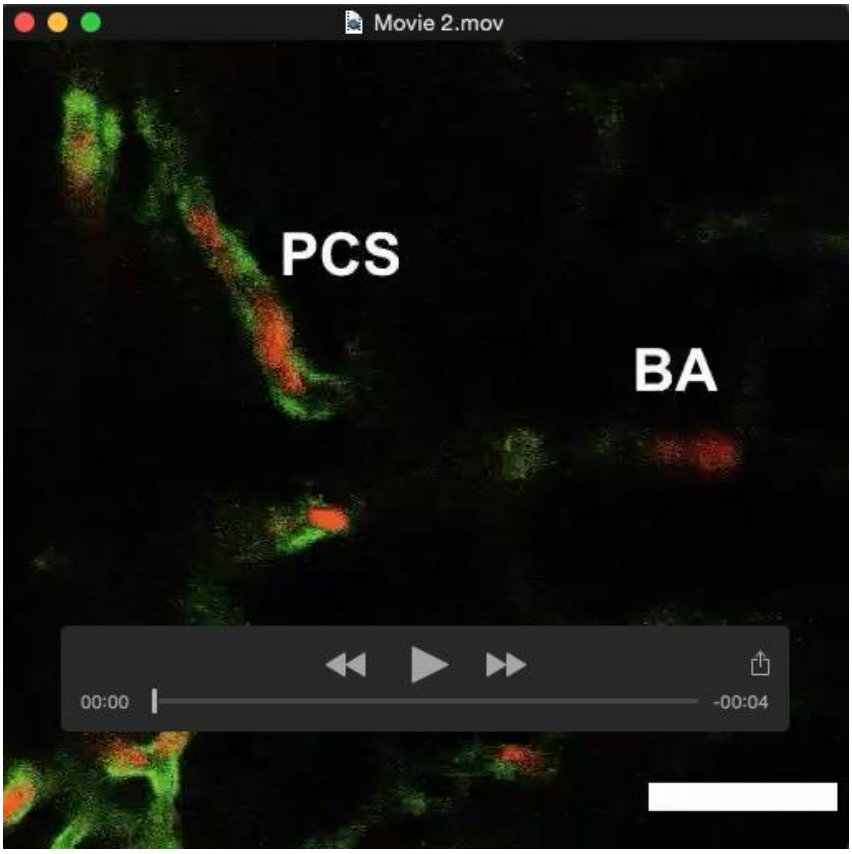

Movie 2. Dorsal view of blood flow through the anterior extra-cerebral Hb vasculature (*reck*^{y72}, 2 dpf). Representative confocal time-lapse movie (10 frames/s); single plane. Anterior, left. Left side, bottom. Endothelium, green (*Tg(kdrl:EGFP)*^{la116}); erythrocytes, red (*Tg(gata1a:DsRed)*^{sd2}). Blood flows through the PCS and BA. Scale bar: 85 µm.

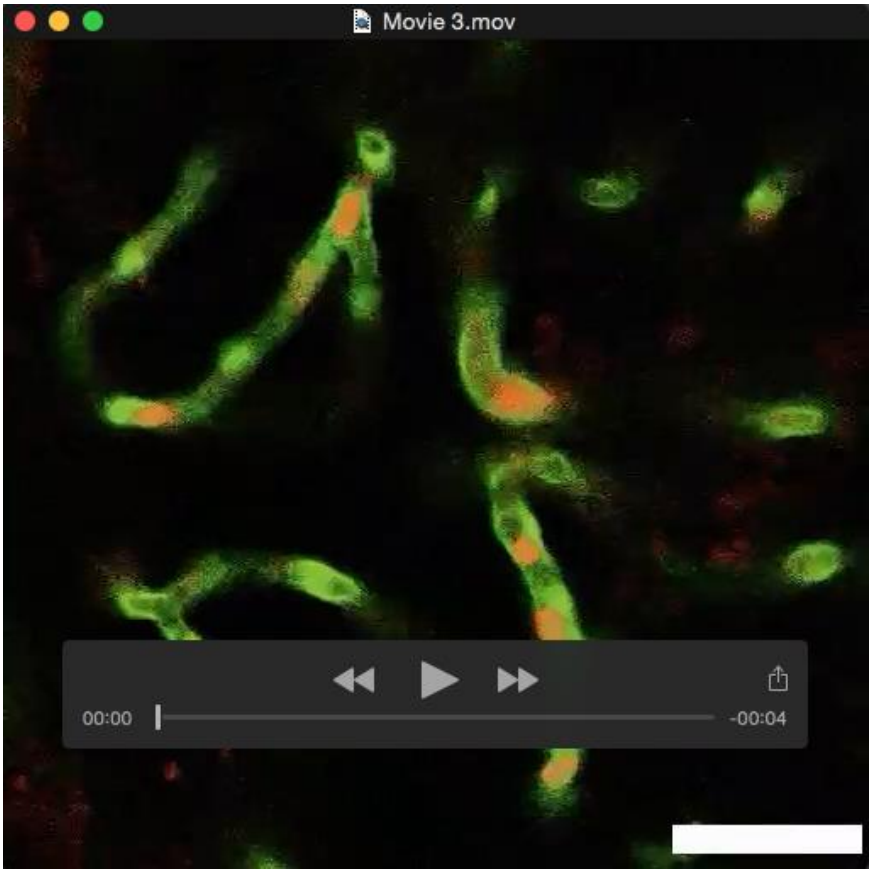

Movie 3. Dorsal view of blood flow through the anterior intra-cerebral Hb vasculature (WT, 2 dpf). Representative confocal time-lapse movie (10 frames/s); single plane. Anterior, left. Left side, bottom. Endothelium, green (*Tg(kdrl:EGFP)*^{la116}); erythrocytes, red (*Tg(gata1a:DsRed)*^{sd2}). Blood flows through CtAs. Scale bar: 85 µm.

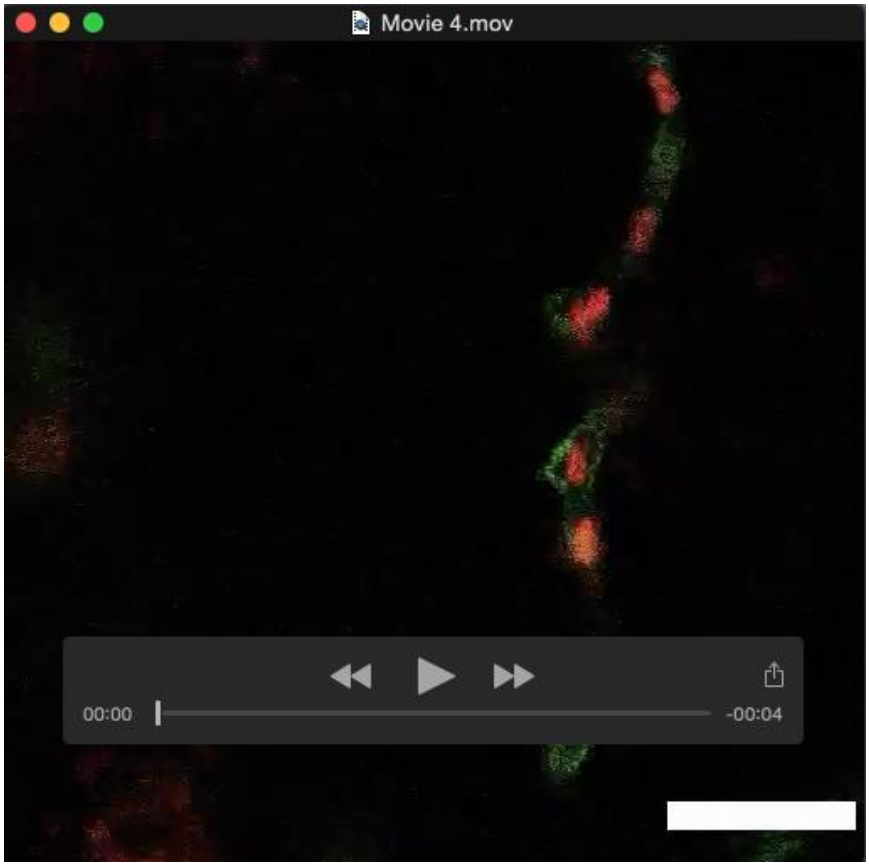

Movie 4. Dorsal view of blood flow through the anterior intra-cerebral Hb vasculature (*reck*^{y72}, 2 dpf). Representative confocal time-lapse movie (10 frames/s); single plane. Anterior, left. Left side, bottom. Endothelium, green (*Tg(kdrl:EGFP)*^{la116}); erythrocytes, red (*Tg(gata1a:DsRed)*^{sd2}). Blood flows through the two CtAs of this mutant. Scale bar: 85 µm.

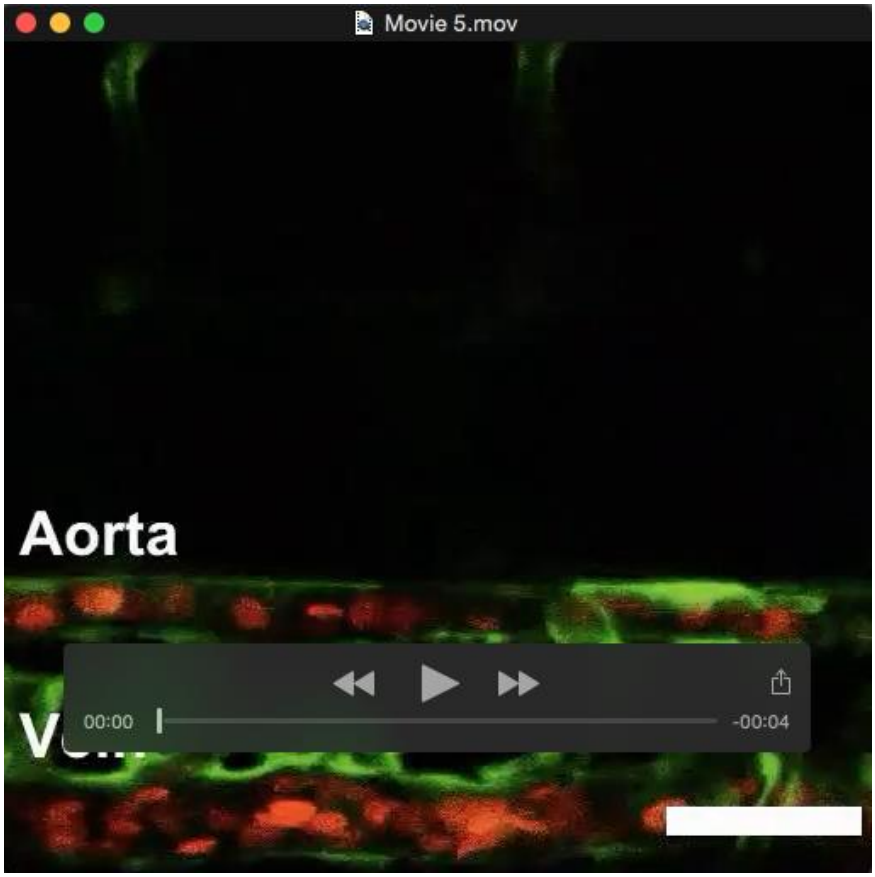

Movie 5. Lateral view of blood flow through the trunk vasculature (WT, 2 dpf). Representative confocal time-lapse movie (10 frames/s); single plane. Anterior, left. Dorsal, up. Endothelium, green (*Tg(kdrl:EGFP)*^{la116}); erythrocytes, red (*Tg(gata1a:DsRed)*^{sd2}). Blood flows through axial (Aorta and Vein; bottom) and Se vessels (unmarked; top). Scale bar: 85 µm.

Movie 6. Lateral view of blood flow through the trunk vasculature (*reck*^{y72}, 2 dpf). Representative confocal time-lapse movie (10 frames/s); single plane. Anterior, left. Dorsal, up. Endothelium, green (*Tg(kdrl:EGFP)*^{la116}); erythrocytes, red (*Tg(gata1a:DsRed)*^{sd2}). Blood flows through axial (Aorta and Vein; bottom) and Se vessels (unmarked; top right quadrant). Scale bar: 85 µm.

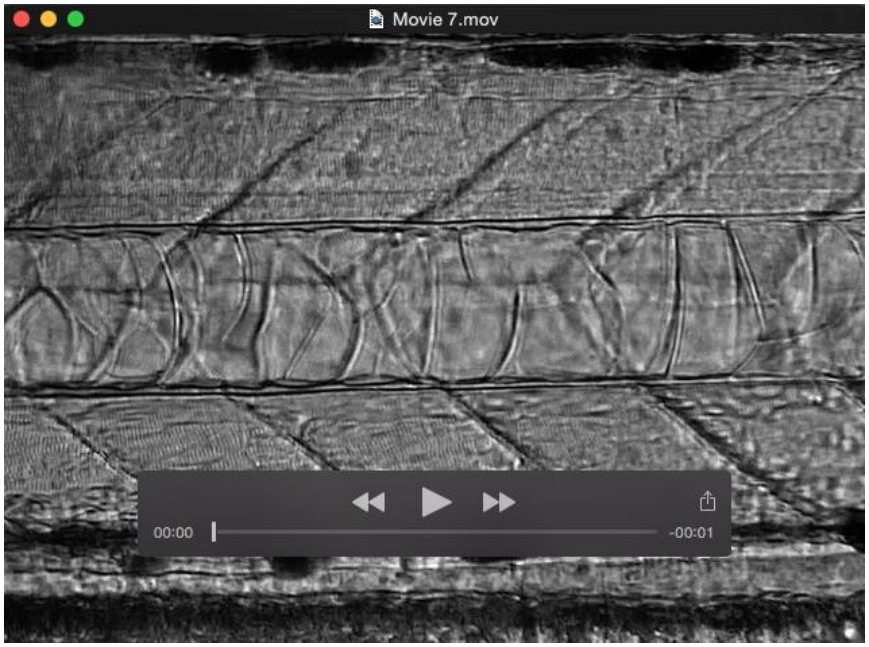

Movie 7. Lateral view of blood flow through the trunk vasculature (*reck*^{y72}, 3 dpf). Representative brightfield time-lapse movie (30 frames/s); single plane. Anterior, left. Dorsal, up. Blood flows through axial (Aorta and Vein) and Se vessels. Image size: W 740 x H 540 µm.

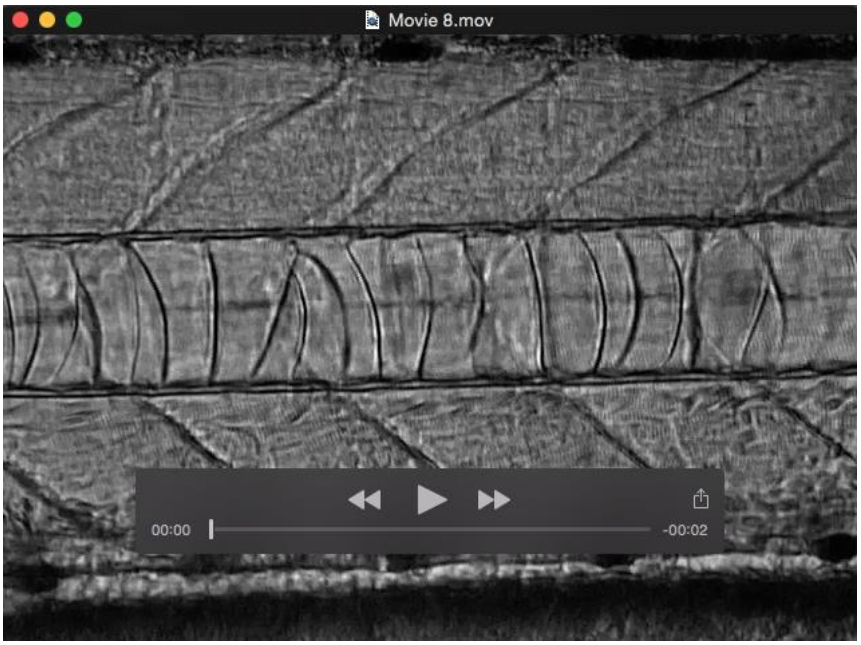

Movie 8. Lateral view of blood flow through the trunk vasculature of a WT sibling (from *reck*^{y72} in-cross; 3 dpf). Representative brightfield time-lapse movie (30 frames/s); single plane. Anterior, left. Dorsal, up. Blood flows through axial (Aorta and Vein) and Se vessels. Image size: W 740 x H 540 µm.

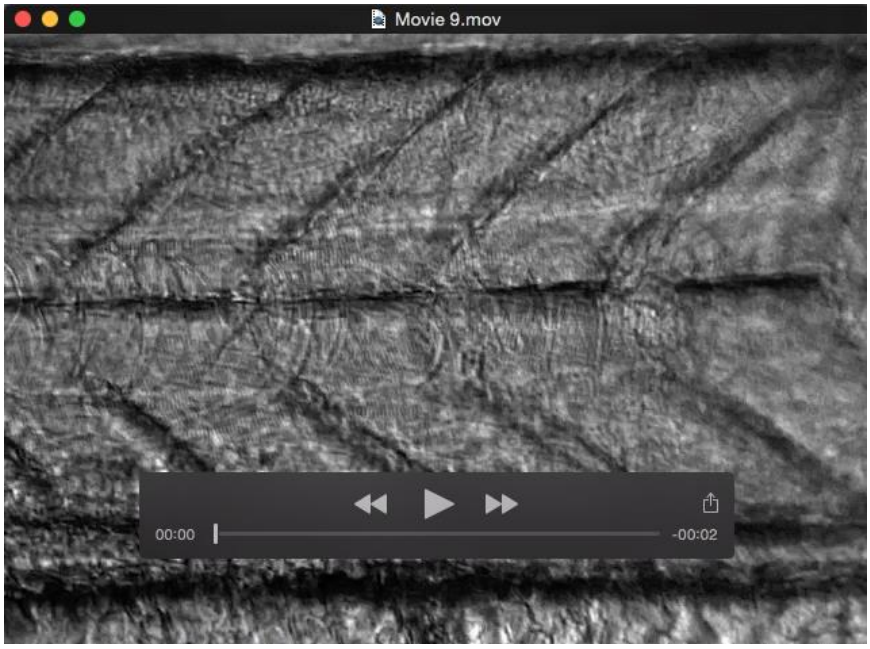

Movie 9. Lateral view of blood flow through the trunk vasculature (*Df(Chr24:reck)*^{w15}; 3 dpf). Representative brightfield time-lapse movie (30 frames/s); single plane. Anterior, left. Dorsal, up. Blood flow is absent. Image Size: W 740 x H 540 µm.

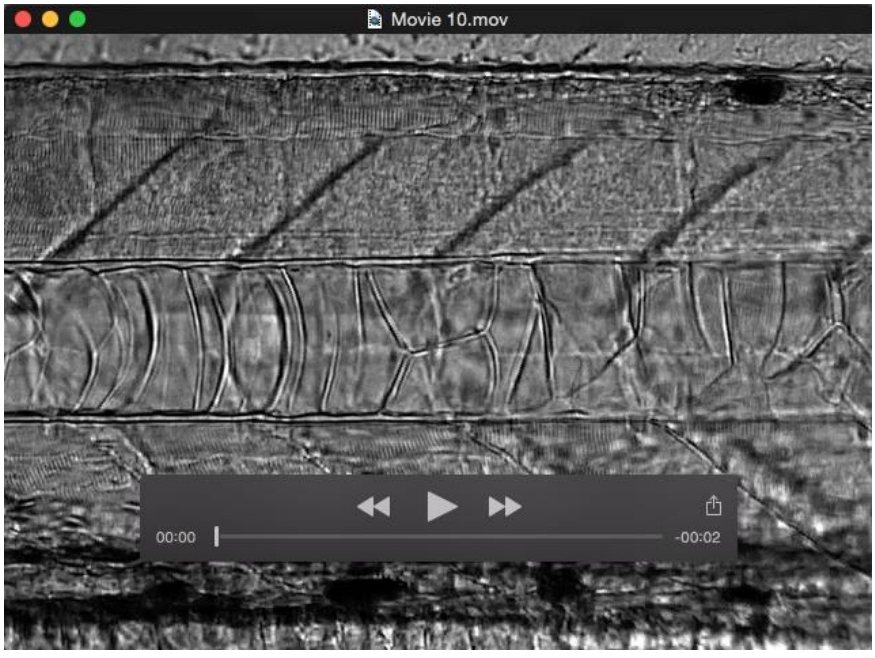

Movie 10. Lateral view of blood flow through the trunk vasculature of a WT sibling (from *Df(Chr24:reck)*^{w15} in-cross; 3 dpf). Representative brightfield time-lapse movie (30 frames/s); single plane. Anterior, left. Dorsal, up. Blood flows through axial (Aorta and Vein) and Se vessels. Image Size: W 740 x H 540 µm.

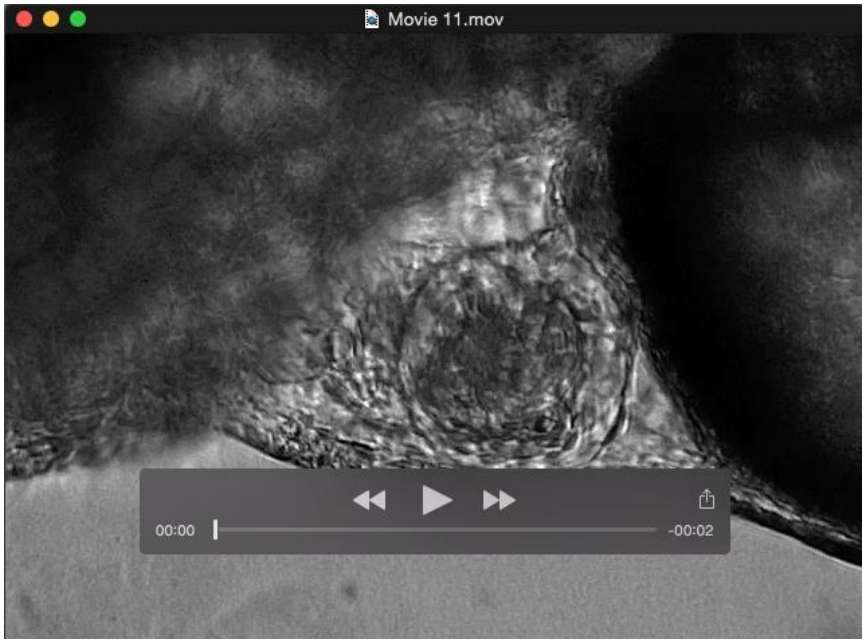

Movie 11. Cardiac contractility and circulation near the heart (*reck*^{y72}, 3 dpf). Representative brightfield time-lapse movie (30 frames/s); single plane. Anterior, left. Dorsal, up. Blood flows and cardiac contractility appears normal. Image Size: W 740 x H 540 µm.

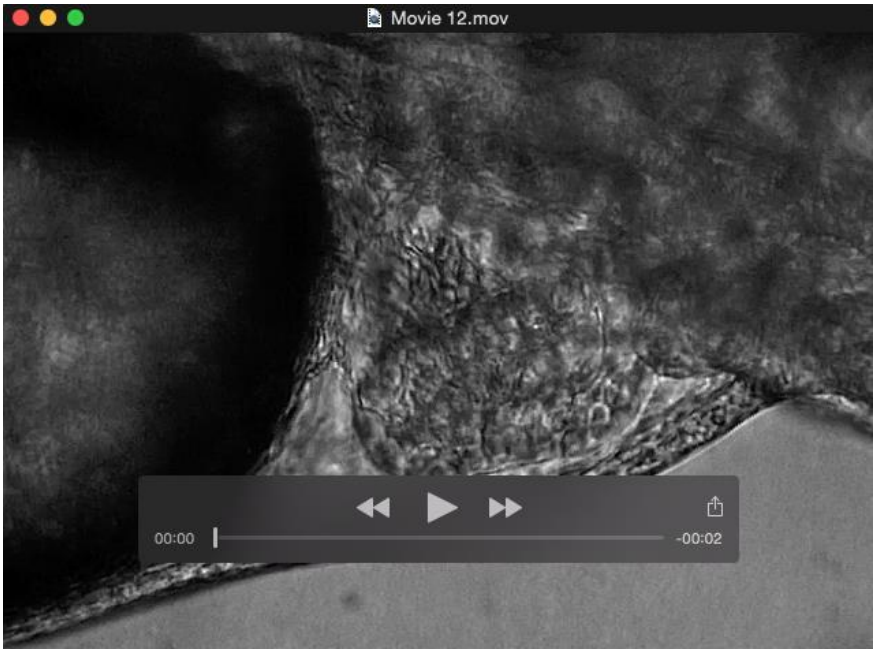

Movie 12. Cardiac contractility and circulation near the heart (WT sibling from *reck*^{y72} in-cross, 3 dpf). Representative brightfield time-lapse movie (30 frames/s); single plane. Anterior, left. Dorsal, up. Blood flows and cardiac contractility appears normal. Image Size: W 740 x H 540 µm.

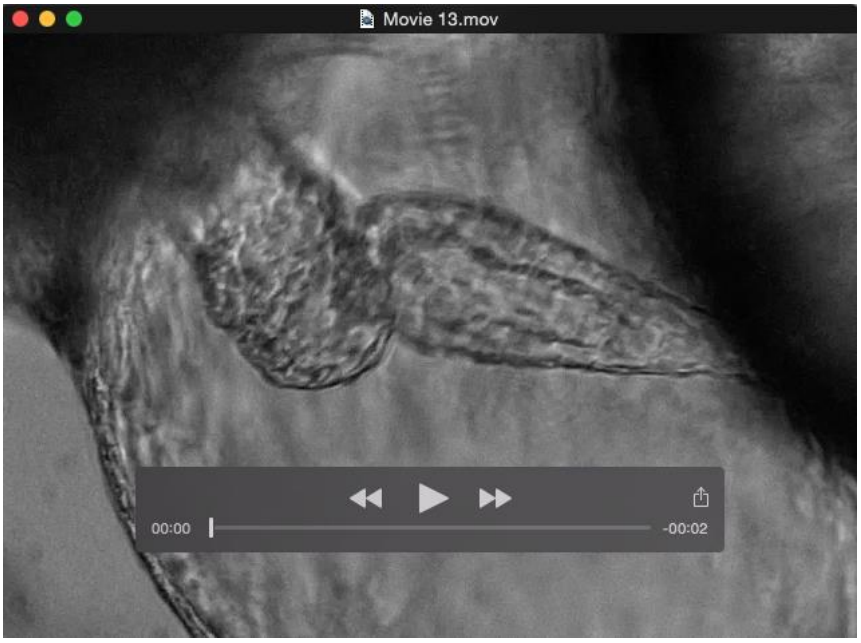

Movie 13. Cardiac contractility and circulation near the heart (*Df(Chr24:reck)*^{w15}; 3 dpf). Representative brightfield time-lapse movie (30 frames/s); single plane. Anterior, left. Dorsal, up. Note misshapen contracting heart and blood flow absence. Image Size: W 740 x H 540 µm.

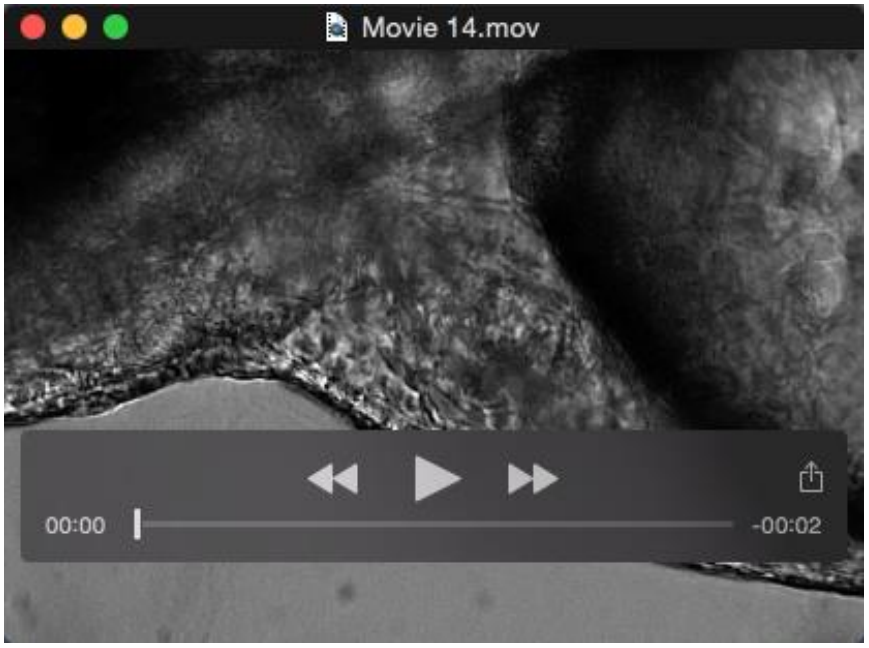

Movie 14. Cardiac contractility and circulation near the heart (WT sibling from *Df(Chr24:reck)*^{w15} in-cross; 3 dpf). Representative brightfield time-lapse movie (30 frames/s); single plane. Anterior, left. Dorsal, up. Blood flows and cardiac contractility appears normal. Image Size: W 740 x H 540 µm.

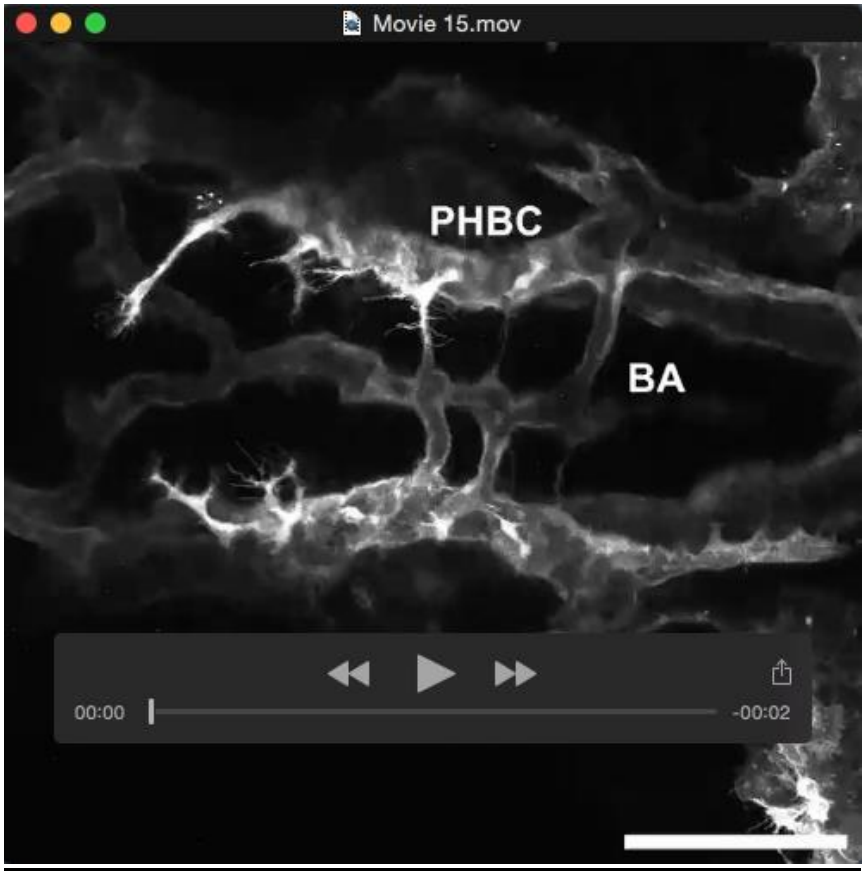

Movie 15. Dorsal view (ventral level) of proper avc dynamics and CtA sprouting in the Hb vasculature (WT; from 33-43 hpf). Representative confocal time-lapse movie (hourly intervals). Anterior, left. Left side, bottom. Endothelium, white (*Tg(kdrl:RFP)*^{s896}). Scale bar: 100 μm. See Fig. S4A-D for avc and CtA sprout labeling.

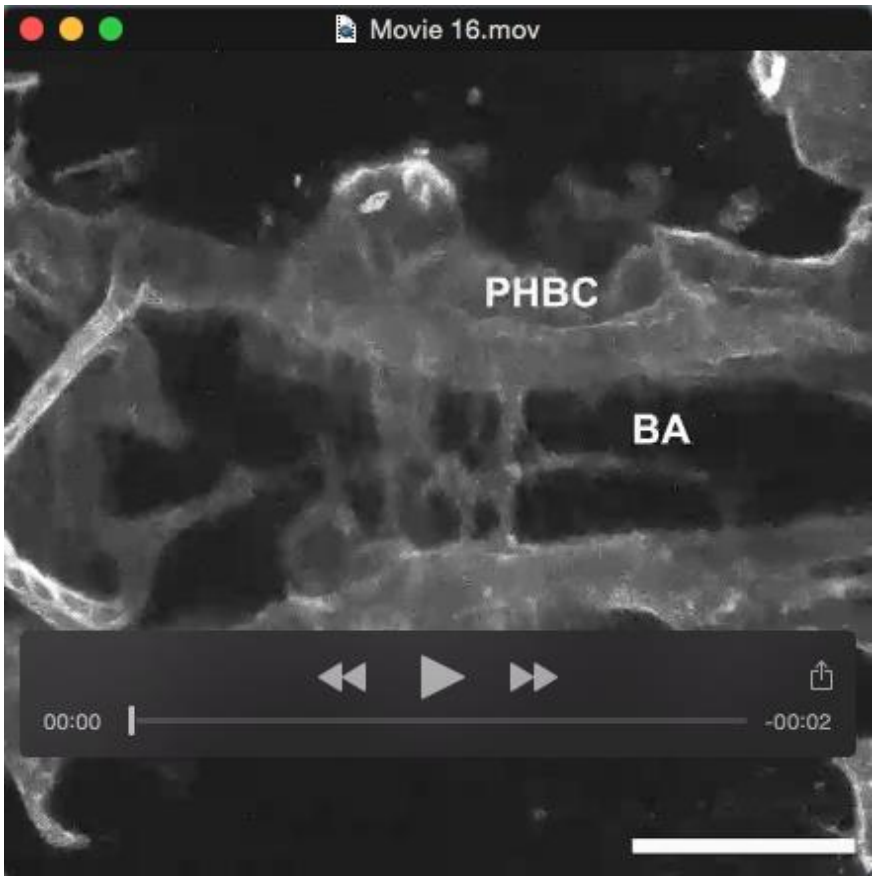

Movie 16. Dorsal view (ventral level) of aberrant avc dynamics and lack of CtA sprouting in the Hb vasculature (*reck*^{y72}; from 33-45 hpf). Representative confocal time-lapse movie (hourly intervals). Anterior, left. Left side, bottom. Endothelium, white (*Tg(kdrl:RFP)*^{s896}). Scale bar: 100 µm. CtA sprouts are not observed. See Fig. S4E-H for avc labeling.

SUPPLEMENTARY MATERIALS AND METHODS

Zebrafish genotyping

kdrl^{y17}: We PCR-amplified a 320 bp genomic fragment using y17-F (5'-GCTTCTGTCGTTCATTCTTAA-3') and y17-R (5'-ACTAAAGATAACCTGTTACAGTTACCTCTC-3') primers. The product was digested with DdeI and run on a 3.5% agarose TBE gel. The WT allele is cut twice, yielding a visible 270 bp fragment and two smaller undetectable fragments. The mutant allele is cut only once, resulting in a visible 300 bp fragment and a smaller undetectable fragment. ***reck***^{y72}: We PCR-amplified a 489 bp fragment using y72-F (5'-CTGTCAGCTGGCCTGTAAGCGTATCC-3') and y72-R (5'-GGGGCATACAGTAGCTCCTCCCCT-3') primers. The product was purified and sequenced using the y72-R primer. ***reck***^{w14}: We PCR-amplified a 232 bp fragment using w14-F (5'-CACAGAGCAGGAGATCATGGAC-3') and w14-R (5'-TAAAGCTGCTGTTCTGGGGTAAAG-3') primers. The PCR product was digested with BfaI and ran on a 3.5% agarose TBE gel. BfaI cuts the mutant allele only, yielding 162 and 70 bp fragments. ***sih***^{b109}: This allele contains a 13 bp deletion at the promoter. The mutant allele was diagnosed by its smaller size. PCR products were obtained using the b109-F (5'-GCATAGAAGCCCTTACAACATC-3') and b109-R (5'-GCTGTCGTCTGATAACACG-3') primers and run on a 3.5% agarose TBE gel. The WT product is 123 bp, the mutant is 110 bp.

Whole-mount RNA *in situ* hybridization (WISH)

Vector templates (Torres-lab identifier, #) were used to make anti-sense riboprobes against: *cdh5/ve-cdh* (#287) (Larson et al., 2004), *tie1* (#101) (Lyons et al., 1998), *fli1a* (#100) (Thompson et al., 1998); *dll4* (#592) (Covassin et al., 2009); *kdrl* (#592) (Choi et al., 2007); *cxcr4a* (#794) (Bussmann et al., 2011); *dab2* (#899) (Bussmann et al., 2011); *mmp2* (#917) (Janssens et al., 2013), *mmp14a* (#919*)* (Coyle et al., 2008); *wnt1* (#750) (Heisenberg et al., 1999); *vegfaa* (#896), *vegfab* (#897) (Bussmann et al., 2011), *cxcl12b/sdf1b* (#886) (Fujita et al., 2011); *plvap/vsg1* (#1385) (Siekmann et al., 2009) *glut1/slc2a1* (#1390) (Zheng et al., 2010) and *reck* (#1140) (Prendergast et al., 2012).

HCR *in situ* hybridization

DNA probes (5'-3') against *reck* transcripts (Molecular Instruments): (P1-gcctcacacactgtagagtacgactcgccgttatgagcacacacctcacg, P2-ccgactgcatgacagcggccctgataatccaccgccacacgctccgagaa, P3-tggacagggaacagcgttacagccggagtcagaaccgaactcagactcca, P4-gttcatttgtgctttattccagaggatccgcagcattcctgcacacaccg, P5-ccgagttaatgagggagtcgatcttctctgcttccttactgcaggcttca). Protocol adapted from Choi et al., 2014. Briefly, embryos were fixed for 24h (4% PFA/4ºC), methanol-permeabilized, rehydrated, ProtK-digested (if >30 hpf) and incubated with probes overnight. Probes removed by washing in Wash Buffer/5xSSCT mixes. Embryos were incubated overnight with the fluorescently-tagged amplifier that specifically recognizes the probes, washed in 5xSSCT, mounted and imaged.

Cell culture

Reagents

Recombinant human VEGF165 and SU5416 were purchased from GEMINI BIO-PRODUCTS and SIGMA respectively. Antibodies: pVEGFR-2 (#2478), VEGFR-2 (#2479), pAKT (Ser473) (#4058), AKT (#9272), pERK1/2 (Ser473) (#4370), ERK1/2 (#4695), Reck (#3433), GAPDH (#4058) and HA (# 2367) from Cell Signaling. GFP and FLAG from Life Technologies and SIGMA respectively. Human Umbilical Vein Endothelial Cells (HUVEC) primary cell culture, Human Embryonic Kidney 293T (HEK293T) and COS-7 cell lines were kindly provided by Timothy Hla, Matthias Stadtfeld and Stevan R Hubbard´s laboratories respectively. Control (sc-108080) and human RECK (sc-39718-V) shRNA lentiviral particles from Santa Cruz Biotechnology Inc.

Cell culture

HUVEC cells were grown in low serum medium optimized for the culture of human endothelial cells (Vasculife EnGS VEGF-Free medium, from Lifeline Cell Technology). HEK293T and COS-7 cell lines were maintained in Dulbecco's modified Eagle's medium (DMEM; GIBCO) supplemented with 10% fetal bovine serum (FBS). Cells grown in 10-cm diameter dishes were incubated at 37°C in a humidified atmosphere with 5% CO2.

Lentivirus infection and transfection

1 X 10^5 HUVECs/well were seeded in a 6-well plate covered with 0.1% gelatin (SIGMA). Next day, HUVECs were infected with control or human RECK shRNA lentiviral particles supplemented with 5 µg/ml polybrene (Millipore). 24 h post-infection the medium was changed and HUVECs were selected for 48 h with 10 µg/ml puromycin. Post-selection cells were starved overnight and stimulated with/without VEGF165 (10 ng/mL) for 2 min. HUVECs were used between passages 2-6. HEK 293T or COS-7 (70% confluence) cells grown in 3.5-cm diameter dishes were transfected using Lipofectamine-2000 reagent (Invitrogen) according to the manufacturer's instructions, with 2 µg of epitope-tagged

versions of the WT (^{3xFLAG}Reck or ^{2xHA}Reck) and mutant (^{3xFLAG}Reck^{y72} or ^{2xHA}Reck^{y72}) zebrafish Reck proteins. 3 h post-transfection, the OPTI-MEM medium was replaced with complete DMEM. Cells were used for western blot or immunofluorescence assays at 48 h post-transfection. Western blot assays: *To investigate whether Reck promotes VEGF-A signaling* HUVECs were cultured, infected with shRNA lentivirus particles and stimulated w/wo VEGF165 as described. In some experiments we combined VEGF-A stimulation (10 ng/ml for 2 min) and SU5416 (5 μM for 1h) mediated inhibition of VEGF-A signaling.

Measuring the abundance of WT and mutant epitope-tagged Reck proteins

COS-7 cells were transfected with CMV-driven v**ectors** (Torres-lab identifier, #) for co-expressing epitope-tagged (FLAG or HA) Reck (#1190-1) or Reck^{y72} (1334-5) with EGFP in cultured cells. For whole-cell lysates, cells on 6 well plate were placed on ice, rinsed once with phosphate-buffered saline (PBS), lysed in 0.25 ml of room temperature buffer (20 mM Tris [pH 7.5], 0.5 mM EDTA, 150 mM NaCl, 1 mM EGTA and 1% SDS) containing protease and phosphatases inhibitors (COMPLETE–EDTA Free from Roche) and loaded onto 4-12% Nu-PAGE gels. Proteins were transferred to Immobilon membranes (Millipore), detected by Western blotting and revealed with Western Lightning PLUS-ECL (PerkinElmer). Western Blot densitometry quantification performed with ImageJ software. Experiments were done at least in triplicate.

Immunofluorescence and imaging

The cell surface localization of epitope-tagged versions of WT (3xFLAG-Reck or 2xHA-Reck) and mutant (3xFLAG-Reck^{y72} or 2x-HAReck^{y72}) zebrafish Reck proteins was assayed via immunofluorescence staining of non-permeabilized HEK293T cells. 2 days post-transfection, cells were washed with PBS, fixed with fresh 4% paraformaldehyde in PBS, pH 7.4, for 20 min at room temperature, washed five times with PBS and incubated with 1% bovine serum albumin for 30 min at 37°C. FLAG and HA tags were detected with monoclonal antibodies (1/500) in 0.5% bovine serum albumin for 1 h at 37°C, washed, and followed by incubation with secondary anti-mouse antibody Alexa 546 at 1/500 in 1% bovine serum albumin for 40 min at room temperature. Images of fixed cells were acquired with an inverted Nikon Eclipse Ti-E fluorescence microscope using the 20X objective.

REFERENCES

Brand, M., Heisenberg, C. P., Jiang, Y. J., Beuchle, D., Lun, K., Furutani-Seiki, M., Granato, M., Haffter, P., Hammerschmidt, M., Kane, D. A., et al. (1996). Mutations in zebrafish genes affecting the formation of the boundary between midbrain and hindbrain. *Development* **123**, 179-190.

Coyle, R. C., Latimer, A. and Jessen, J. R. (2008). Membrane-type 1 matrix metalloproteinase regulates cell migration during zebrafish gastrulation: evidence for an interaction with non-canonical Wnt signaling. *Experimental cell research* **314**, 2150-2162.

Heisenberg, C. P., Brennan, C. and Wilson, S. W. (1999). Zebrafish aussicht mutant embryos exhibit widespread overexpression of ace (fgf8) and coincident defects in CNS development. *Development* **126**, 2129-2140.

Kim, C. H., Ueshima, E., Muraoka, O., Tanaka, H., Yeo, S. Y., Huh, T. L. and Miki, N. (1996). Zebrafish elav/HuC homologue as a very early neuronal marker. *Neuroscience letters* **216**, 109-112.

Lowery, L. A., De Rienzo, G., Gutzman, J. H. and Sive, H. (2009). Characterization and classification of zebrafish brain morphology mutants. *Anatomical record* **292**, 94-106.

Siekmann, A. F., Standley, C., Fogarty, K. E., Wolfe, S. A. and Lawson, N. D. (2009). Chemokine signaling guides regional patterning of the first embryonic artery. *Genes & development* **23**, 2272-2277.

Thompson, M. A., Ransom, D. G., Pratt, S. J., MacLennan, H., Kieran, M. W., Detrich, H. W., 3rd, Vail, B., Huber, T. L., Paw, B., Brownlie, A. J., et al. (1998). The cloche and spadetail genes differentially affect hematopoiesis and vasculogenesis. *Developmental biology* **197**, 248-269.

Zheng, P. P., Romme, E., van der Spek, P. J., Dirven, C. M., Willemsen, R. and Kros, J. M. (2010). Glut1/SLC2A1 is crucial for the development of the blood-brain barrier in vivo. *Annals of neurology* **68**, 835-844.

Table S1. *nft^{y72}/sdp* trans-heterozygotes and both *nft^{y72}* and *sdp* homozygotes have identical CtA and DRG deficits. Percentage of embryos (different genotypes) showing indicated defects at specified ages (D2: 2 dpf; D3: 3 dpf) "*w15* sibs (+)" are embryos with CtAs and DRG from a *Df(Chr24:reck)^{w15}*/+ in-cross. A significant percentage of them, like *Df(Chr24:reck)^{w15}* homozygotes, show hemorrhage. *Df(Chr24:reck)^{w15}* homozygotes also show heart edema and circulatory deficits (see also Fig. 1, Figs. S1-3 and Movies 1-14). These defects are rare/absent in other *reck*$^{-}$ genotypes, including heterozygotes of other alleles. Thus, they are likely due to the removal of additional genes in *Df(Chr24:reck)^{w15}*. Notably, *reck* point mutants lack the global vascular defects of *reck* morphants in (Prendergast et al., 2012), which are likely due to morpholino off-target effects; see (Kok et al., 2015; Schulte-Merker and Stainier, 2014) (Stainier et al., 2015) and references therein. In contrast, the vascular phenotypes of *reck* point mutants resemble those of *reck* morphants in (Vanhollebeke et al., 2015).

***n* embryos scored at**		**Genotype**	**Percentage of embryos with**													
			Deficits in the presence of blood vessels						**Defective cardiovascular function**						**DRG deficit**	
			CtAs		**MCeV**		**Se + DLAV**		**Hemorrhage**		**Heart edema**		**Circulation**			
D2	**D3**		**D2**	**D3**	**D2**	**D3**	**D2**	**D3**	**D2**	**D3**	**D2**	**D3**	**D2**	**D3**	**D2**	**D3**
100	100	+/+	0	0	0	0	0	0	0	0	0	0	0	0	0	0
66	134	***w15* sibs (+)**	0	0	0	0	0	0	**27**	**3**	0	0	**2**	**1**	0	0
12	49	***w15 / w15***	**100**	**100**	0	0	0	0	**8**	**27**	0	**100**	**75**	**100**	**100**	**100**
19	40	***y72 / y72***	**100**	**100**	0	0	0	0	**5**	**5**	0	0	0	0	**100**	**100**
36	13	***y72 / w15***	**100**	**100**	0	0	0	0	**8**	0	**3**	0	0	0	**100**	**100**
10	10	***y72 / w14***	**100**	**100**	0	0	0	0	0	0	0	0	0	0	**100**	**100**

Table S2. *reck* limits avc abundance even without circulatory flow. Average Abundance (A) for different vessels in the indicated genotypes. n=10 embryos per genotype (50 hpf) analyzed via confocal imaging. SD, Standard deviation. Statistical significance calculated with Student's *t*-test. Pairs of genotypes with significant differences between them indicated with a plus "+" sign. Non-significant differences indicated with "NS". See also Fig. S5.

Vessels	**Genotype**								**Pairs of genotypes with significant differences (p <0.05)**					
	WT		***sih^{b109}***		***reck^{y72}***		***reck^{y72}; sih^{b109}***		**WT**			***sih^{b109}***		***reck^{y72}***
	A	SD	**A**	SD	**A**	SD	**A**	SD	***sih^{b109}***	***reck^{y72}***	***reck^{y72}; sih^{b109}***	***reck***	***reck^{y72}; sih^{b109}***	***reck^{y72}; sih^{b109}***
avc between PHBC-BA	**0.1**	0.3	**3.4**	1.7	**3.6**	1.7	**10.4**	2.1	+	+	+	**NS**	+	+
avc between PHBC-PCS	**0.2**	0.4	**0.2**	0.4	**3.2**	1.3	**1.8**	1.1	**NS**	+	+	+	+	+
avc TOTAL	**0.3**	0.5	**3.6**	1.7	**6.8**	1.8	**12.2**	2.3	+	+	+	+	+	+
CtAs	**11.4**	1.6	**11.1**	2.4	**2.0**	0.8	**0.9**	1.0	**NS**	+	+	+	+	+